



Original Paper

Three-Dimensional Integrated Geo-Static Modeling for Prospect Identification and Reserve Estimation in the Middle Miocene Multi-Reservoirs: A Case Study from Amal Field, Southern Gulf of Suez Province

Mohammed Amer ^{1,2} Walid M. Mabrouk,¹ Khaled S. Soliman,¹ Ahmed M. Noureldin,¹ and Ahmed Metwally¹

Received 15 March 2023; accepted 13 August 2023
Published online: 8 September 2023

Middle Miocene reservoirs in the southern part of the Gulf of Suez province are characterized by geometrical uncertainties due to their structural settings, lateral facies change, different lithologies, and diverse reservoir quality. Therefore, in this study, detailed 3D geo-static models were constructed by integrating multiple datasets, including 2D seismic sections and digital well-logs. The 3D models were constructed for the Belayim Formation (Hammam Faraun Member), Kareem Formation (Markha Member), and Rudies Formation (Upper Rudies Member) with detailed structuration, zonation, and layering for Amal Field in the southern Gulf of Suez province to assess the hydrocarbon potential, calculate accurate reserves, recommend development and exploration plans, and propose locations for future drilling. The resultant structural model exhibited a compartmentalized area of major and minor normal faults trending NW–SE, forming structurally high potential hydrocarbon trapping locations in the study area. The petrophysical models indicated the good potentiality of Hammam Faraun as a reservoir with porosity values of 15–23%, increasing towards the central part of the area, volume of shale (V_{sh}) of 21–31%, water saturation (S_w) of 34–49%, and sand thickness increasing toward the northeastern part of the area. The Markha Member was also interpreted as a good reservoir, with porosity values of 15–22%, increasing towards the southeastern part of the area, V_{sh} of 13–29%, S_w of 16–38%, and sandy facies accumulating in the central horst block. Upper Rudies exhibits good reservoir properties with porosity values of 16–23%, V_{sh} of 29–37%, S_w of 35–40%, and good sandy facies in the central horst block of the area. The study results showed hydrocarbon potential in the central horst block of the study area for the Middle Miocene multi-reservoirs.

KEY WORDS: Seismic interpretation, 3D geo-static model, Reserve estimation, 3D petrophysical modeling, Facies modeling, Southern Gulf of Suez.

INTRODUCTION

The 3D static modeling of producing reservoirs is very important to control the proper evaluation for the exploration and development phases. A variety of geoscience platforms can be used to model hydrocarbon reservoirs (Abdel-Fattah et al., 2010,

¹Geophysics Department, Faculty of Science, Cairo University, Giza 12613, Egypt.

²To whom correspondence should be addressed; e-mail: mohamedamer@cu.edu.eg

2018; Nouredin et al., 2023a, 2023b, 2023c, 2023d). However, the accuracy of the modeling process is still a major challenge that can affect the development of reservoirs (Bryant & Flint, 1992; Bilodeau et al., 2002; Nouredin et al., 2023a, 2023b, 2023c, 2023d).

A 3D structural model is obtained based on seismic interpretation outputs (Abdelmaksoud et al., 2019a, 2022; Radwan et al. 2022), which include depth maps and associated fault sticks/planes. The ability to construct complex structures is a main advantage of a 3D structural model. Moreover, it enables the interpreter to inspect and analyze the static model (Fagin, 1991) by showing a variety of geological cross-sections of the model in any direction (Cosentino, 2005), and the seismic world is linked to other branches of structural geology via the structural model (De Jager & Raymond, 2006). The advantage of modeling complex hydrocarbon reservoirs with varying formations and reservoir heterogeneity is the fundamental benefit of 3D modeling methodologies (Radwan et al., 2022). Therefore, correct parameters and the integration of the best data are necessary for superior reservoir modeling (Nouredin et al., 2023a, 2023b, 2023c, 2023d).

There should be some caution when determining rock and petrophysical properties from electrical well logs (Radwan et al., 2020; Nouredin et al., 2023a, 2023b, 2023c, 2023d). There may be uncertainties associated with geological, seismic, and petrophysical interpretations in the geo-evaluation processes. Therefore, the best-fit parameters were used in the reservoir static modeling to decrease the final geological model uncertainties. The ability to model complex structures is a primary benefit of 3D modeling approaches. By displaying cross sections across a built-in model in any direction, this technique enables the interpreter to assess the model. The 3D facies/petrophysical modeling is also essential for linking wellbore parameters to a 3D geo-static model (De Jager and Pols, 2006; Abdel-Fattah et al., 2010; Abdelmaksoud et al., 2019b).

Middle Miocene sediments have excellent hydrocarbon potentiality as a source, reservoir, and seal rocks (Attia et al., 2015; Radwan et al., 2019). The Middle Miocene succession in the Gulf of Suez province is composed of six formations, namely, from base to top: Nukhul, Rudeis, Kareem, Belayim, South Gharib, and Zeit Formations. The sandstones of these formations have good quality and good history of hydrocarbon accumulation. The Nukhul

Formation is composed of marine calcareous conglomerates, sandstones, and marl. The Rudeis Formation is composed of deep marine shale and marl sedimentation with siliciclastic sandstones. The Kareem Formation is subdivided into two members: the lower one is the Markha Member, which is composed of interbedded shale, carbonates and anhydrite with sandstone in the lower part; the upper member is the Shagar, which is composed of shale and marl with thin beds of limestone and sandstone. The Belayim Formation is composed of four members: Hammam Faraun (top), Feiran, Sidri, and Baba (bottom). The Hammam Faraun Member consists of sandstone with shale intercalations. The Feiran, Sidri, and Baba Members consist of evaporite deposits (Bosworth & McClay, 2001; Al-sharhan, 2003; Nabawy and Barakat, 2017; Radwan et al., 2021).

The goal of this study was to construct a detailed 3D geo-static model for the Middle Miocene reservoirs in the Amal Field in the southern Gulf of Suez province, as these reservoirs exhibit different connectivity and geometry, which, in turn, affect the production performance behavior through the life of the field, and are characterized by uncertainties due to their structural settings, lateral facies change, and different lithologies. A 3D model can help to solve these reservoirs problems.

GEOLOGICAL SETTING

The Gulf of Suez rift basin was formed in the late Oligocene – early Miocene (Hempton, 1987; Bosworth et al., 2005). The Gulf of Suez is composed of three major half-grabens that have reversed dip polarity from north to south (Kassem et al., 2020). The major faults of the half-grabens in the north and south dip toward the northeast (Radwan et al., 2021), and the layers within the tilted fault block dip toward the southwest. The major faults of the central half-graben dip toward the southwest, which is the opposite direction relative to the other grabens, and the layers dip toward the northeast (Patton et al., 1994). Two accommodation zones separate the three half-grabens (Moustafa, 1976) (Fig. 1).

Stratigraphically, the Gulf of Suez comprises rocks ranging from Precambrian to Holocene (Said, 1990); these rocks were classified based on tectonic rifting into three stratigraphic phases (Moustafa, 1976) (Fig. 2). The pre-rift stratigraphic phase (pre-Miocene units) rests unconformably on basement

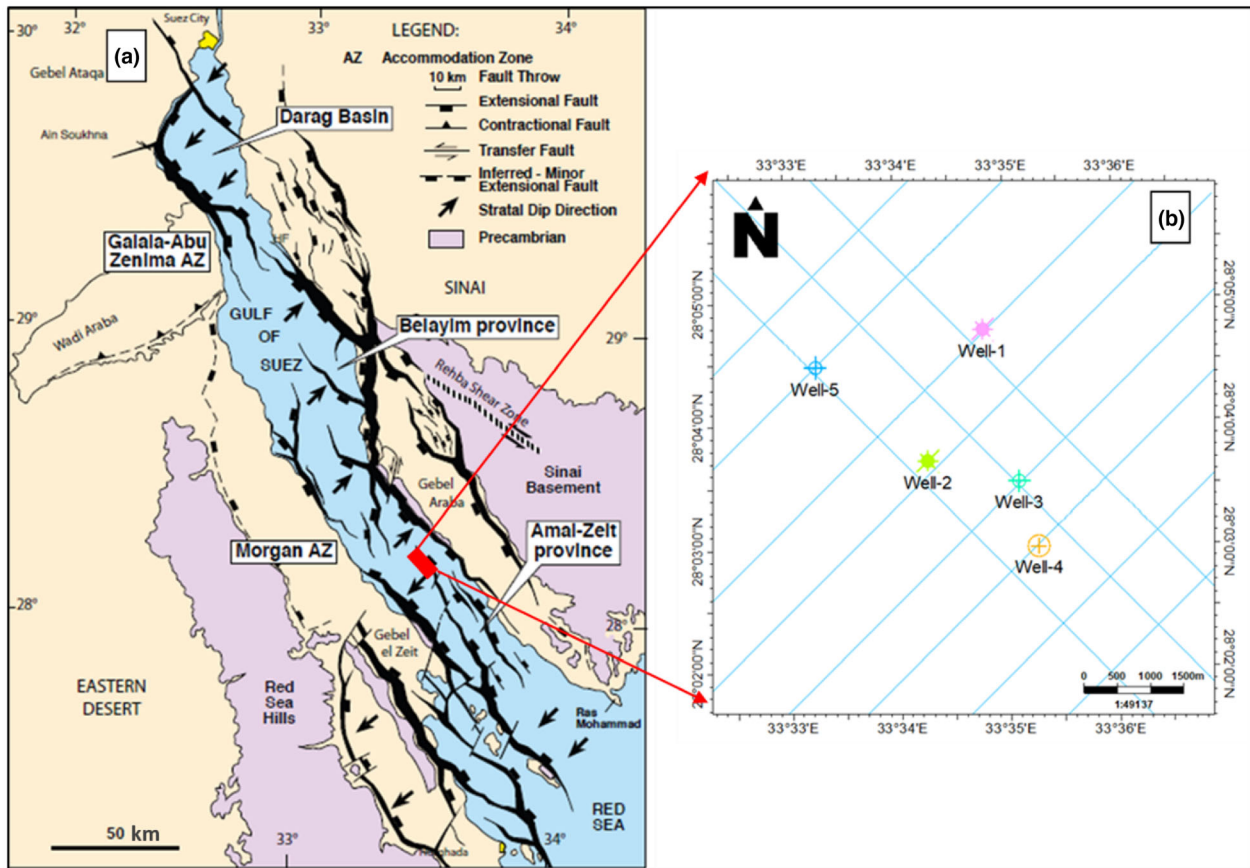


Figure 1. Location map of the study area. (a) Gulf of Suez rift tectonic map (modified after Khalil, 1998). (b) Base map showing the available seismic lines and the five used well locations over the Amal field.

rocks with ages ranging from Paleozoic to Eocene (Alsharahn, 2003). The syn-rift stratigraphic phase (Miocene units) is composed of sedimentary clastic units (Colletta et al., 1988) at the base of the section and evaporitic facies at the top. The post-rift stratigraphic phase (post-Miocene units) includes clastic rock units (Afifi, 2016).

Middle Miocene reservoirs represent approximately 20% of the Gulf of Suez’s production (Patton et al., 1994). Source rocks in the study area may be from the Lower Miocene Rudeis and Kareem Formations and pre-rift units such as the shale of the Thebes Formation, the brown limestone of the Sudr Formation, and the shale of the Matulla Formation (Alsharahn, 2003). The Rudeis Formation may be an oil-prone source rock or an oil and gas-prone source rock (Afifi, 2016). Vertical and lateral evaporites and mudstone represent the cap rocks in the study area. The mode of migration in the study area is

hydrocarbon migration along faults or migration vertically from shale/carbonate source rocks. The trapping mechanism in the study area is fault-bounded horst, and a three-way dip-closed fault-bounded trap (Alsharahn, 2003).

The study area is located between latitudes 28° 02’ N and 28° 05’ N and between longitudes 33° 33’ E and 33° 36’ E (Fig. 1). This study focused mainly on Middle Miocene reservoirs, namely, the Belayim Formation, with more focus on the Hammam Faraun zone, the Markha Member of the Kareem Formation (Patton et al., 1994), and the Upper Rudies Formation. The Hammam Faraun is composed of sandstone, shale intercalations, carbonate, and thin beds of anhydrite. The Markha Member is composed of shales and sandstone intercalations. The Upper Rudies Formation is composed mainly of shales with sandstone units (Alsharahn, 2003; Shehata et al., 2021).

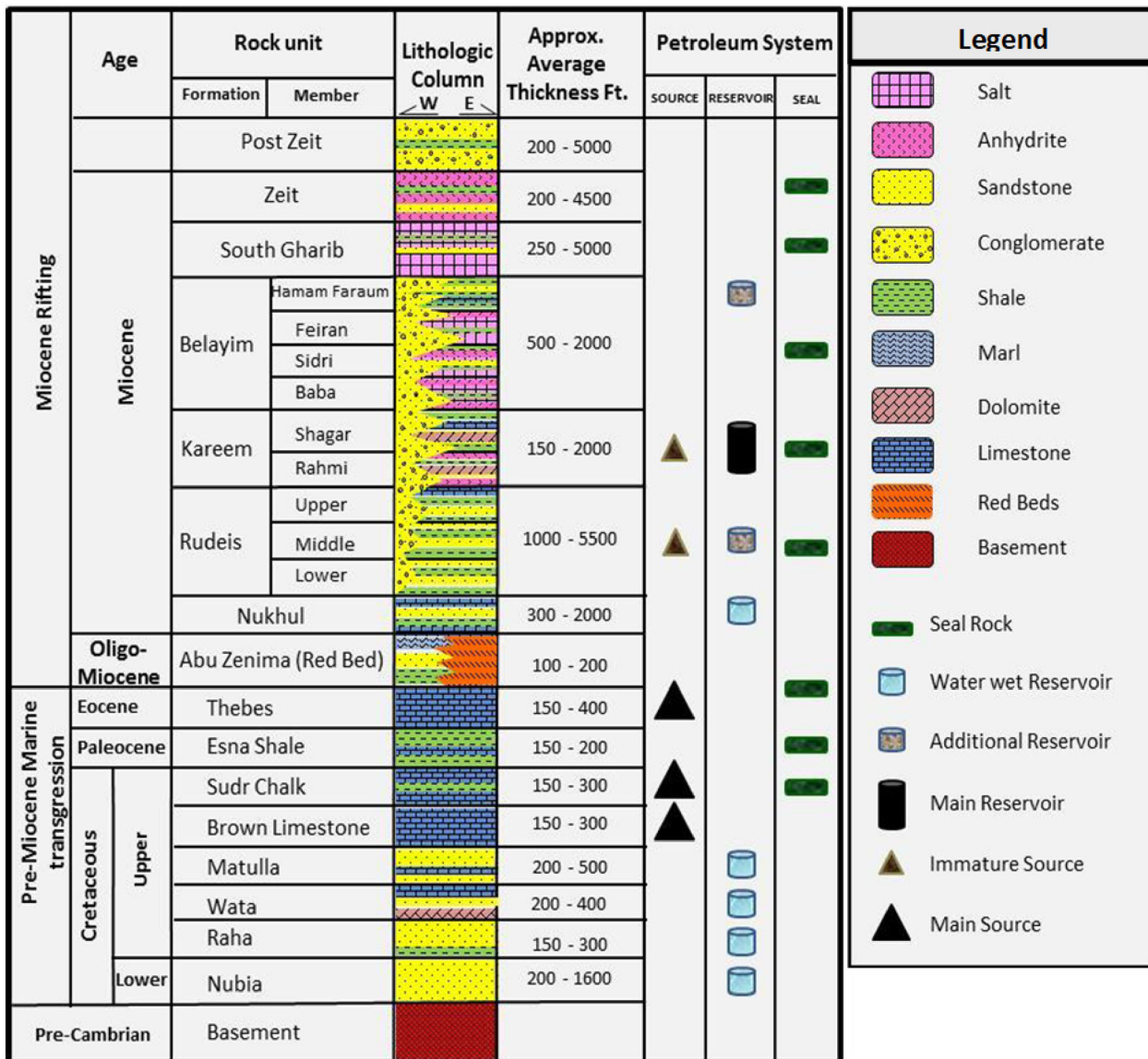


Figure 2. Stratigraphic column of the southern part of the Gulf of Suez (Mostafa et al., 2015).

MATERIAL AND METHODOLOGY

Ten 2D seismic lines in the depth domain along with logging data from five wells (Well #1, #2, #3, #4, and #5), including gamma ray (GR), density, neutron, sonic, and resistivity, were combined for the 3D geo-static modeling of the Belayim Formation (Hammam Faraun Member/zone), Kareem Formation (Markha Member/zone), and Rudies Formation (Upper Rudies Member/zone). Throughout the 3D modeling procedures, several simulation ap-

proaches, such as the sequential Gaussian simulation technique (Hu & Le Ravalec-Dupin, 2005), were proposed to comprehend and model the reservoirs of interest.

The lithology identification of the three main formations was constructed based on four wireline logs: (GR, density, neutron, and sonic). Three sand isolith maps were constructed for the three formations based on the sand net thickness of each reservoir in all the wells, which is constructed based on the interpretation of the log responses. The GR

log was used to differentiate between the shale and non-shale zones, and the other logs were used for the lithology identification of non-shale zones. Sandstone was interpreted based on the low GR and density–neutron crossover. Anhydrite was interpreted mainly based on the high density and high sonic velocity, and salt was interpreted based on low density and low sonic values (Fig. 4).

Seismic data interpretation was initiated by tracking seismic reflectors and structural elements (Noureldin et al., 2023a, 2023b, 2023c) in the depth domain laterally for the mapping of subsurface structure, stratigraphy, and reservoir geometry (Nanda et al., 2016; Abuzaied et al., 2019). The main objective was to discover oil and gas accumulations, track their lateral extent, and estimate their amounts (Avseth et al., 2010; Mahmoud et al., 2023; Nour-eldin et al., 2023a, 2023b, 2023c).

The procedures undertaken in this study were subdivided into various stages, starting with well correlations, seismic interpretation, structural, facies, and petrophysical analysis, then modeling, and ending with the final interpreted model (Radwan et al., 2022). The seismic interpretation outputs were used as input data in fault modeling, pillar gridding, and horizon modeling. The fault modeling step represents the basis for 3D grid generation, followed by the creation of pillar grids, which represent a structural grid created based on fault modeling concerning the horizons of interest. The seismic data were the container for the 3D geologic modeling (facies and their petrophysical characteristics). Figure 3 represents the flowchart for the modeling process.

Facies modeling is significant during the exploration and development phases because it helps to understand facies distribution and reservoir parameters away from known well locations (Radwan et al., 2022). Reservoir variability and hydrocarbon flow can be identified using 3D facies modeling and reservoir geometry (Cressie, 1990). Also, the connectivity of reservoirs represents an important role (Zhang et al., 2019). Gaussian distribution algorithms were used to create simulations of geological properties or to create interpolation that is based on geostatistical techniques (Goovaerts, 1997).

Petrophysical analysis was performed to estimate the key parameters that are used for the evaluation of reservoir characteristics. Wireline logs

were used to evaluate the petrophysical properties of the reservoirs. The key parameters of formations (shale volume (V_{sh}) total porosity, effective porosity, and water saturation (S_w)) were estimated using standard techniques.

The V_{sh} was calculated from GR logs, thus (Asquith and Gibson, 1982):

$$V_{sh} = \frac{GR_{log} - GR_{min}}{GR_{max} - GR_{min}} \quad (1)$$

where V_{sh} is clay or shale volume, GR_{log} is log value of GR, GR_{min} is minimum value of GR, and GR_{max} is maximum value of GR. The V_{sh} was calculated using GR logs for the Hammam Faraun, Markha, and Upper Rudies zones. V_{sh} log curves were scaled up using arithmetic computation. A sequential Gaussian simulation algorithm was used to distribute V_{sh} among and around the wells.

Total porosity was calculated from density and neutron logs using (Eq. 2) after (Asquith and Gibson, 1982), effective porosity was calculated based on total porosity and V_{sh} using (Eq. 3) (Asquith & Gibson, 1982; Stephens et al., 1998).

$$\varnothing_T = \frac{\varnothing_N + \varnothing_D}{2} \quad (2)$$

$$\varnothing_{eff} = \varnothing_T - (V_{sh} * \varnothing_{sh}) \quad (3)$$

where \varnothing_T is total porosity, \varnothing_N is neutron porosity, \varnothing_D is density porosity, \varnothing_{eff} is effective porosity, and \varnothing_{sh} is shale porosity.

The S_w was calculated based on the Indonesian formula because of the presence of shale, thus (Poupon & Leveaux, 1971):

$$\frac{1}{\sqrt{R_t}} = \left[\sqrt{\frac{\varphi^m}{aR_w}} + \frac{V_{cl} \left(\frac{1-V_{cl}}{2}\right)}{\sqrt{R_{cl}}} \right] S_w^n \quad (4)$$

where R_t is true resistivity, V_{cl} is clay or shale volume, a is tortuosity factor, R_w is formation water resistivity, and R_{cl} is resistivity of shale. The S_w was calculated for Hammam Faraun, Markha, and Upper Rudies zones. Using the arithmetic computation, the S_w log was scaled up into the geo-cellular grid of the model. A sequential Gaussian simulation algorithm was used to populate S_w among and around the wells. The outputs of petrophysical analysis are

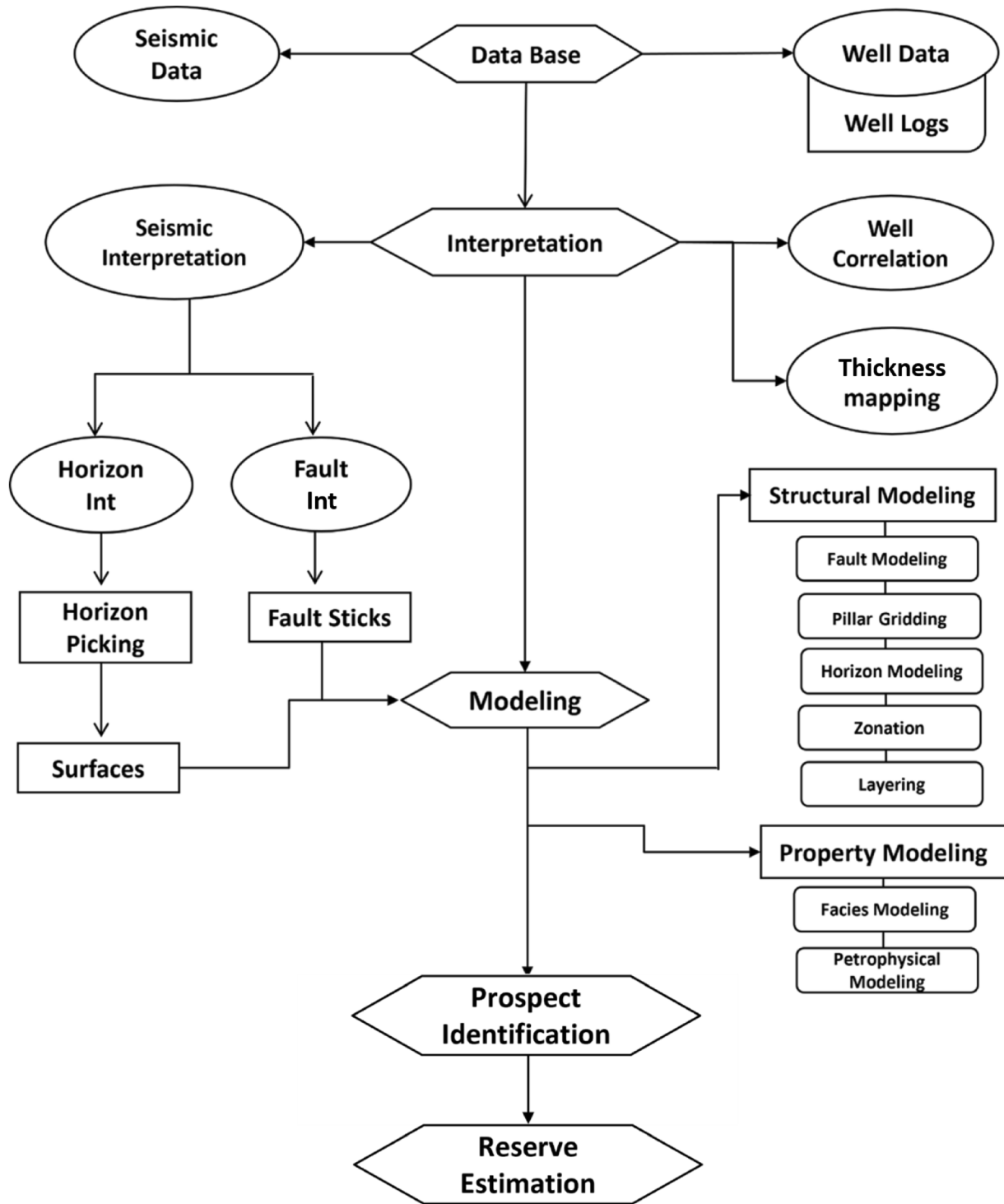


Figure 3. Flowchart for 3D model construction.

used as inputs into the modeling process for the petrophysical parameters of reservoirs.

RESULTS AND DISCUSSION

Well Correlation and Sand Isolith Maps

The correlation was conducted for all the wells based on wireline logs. The correlation chart exhibits three major reservoir intervals with variable thickness throughout the formations of Belayim, Kareem, and Rudies (Fig. 4). The three formations were recorded in all the drilled wells. Three sand isolith maps were constructed for the three formations based on the net thickness of the sand of each reservoir in all the wells.

The Belayim Formation is subdivided into four zones: Hammam Faraun, Feiran, Sidri, and Baba members. The Baba is composed of anhydrite and shale. The Sidri is composed of salt, anhydrite, and shale. The Feiran is composed of anhydrite and shale. The Hammam Faraun is composed mainly of sand and shale intercalations. Sandstone facies are

concentrated in the southeastern part of the area with thickness reaching 34 m (Fig. 5). The thickness distribution varied may be due to the unconformity/erosional surface.

Variable thicknesses of the Kareem Formation were recorded over the study area may be due to unconformity/erosional surface, which is composed of two members, the Markha and Shagar Members. The Shagar Member is composed mainly of shale with minor sand strikes. The Markha is composed of sandstone with shale and streaks of anhydrite. The sandstone thickness of the Markha Member in the southern part of the area is about 60 m (Fig. 6).

The Upper Rudies is composed mainly of shale and sandstone. Sandstones and shales of the Upper Rudeis Member extended over the entire area laterally with thickness variations with 70 m average thickness, ranging from 30 to 120 m thick due to structuration during the deposition that is related to the Kareem–Rudeis unconformity (Okeil et al., 2019). In the southern part of the study area, sandstone thickness reaches about 30 m, according to the sand-isolith map (Fig. 7). The correlation results are in agreement with those of Okeil et al. (2019).

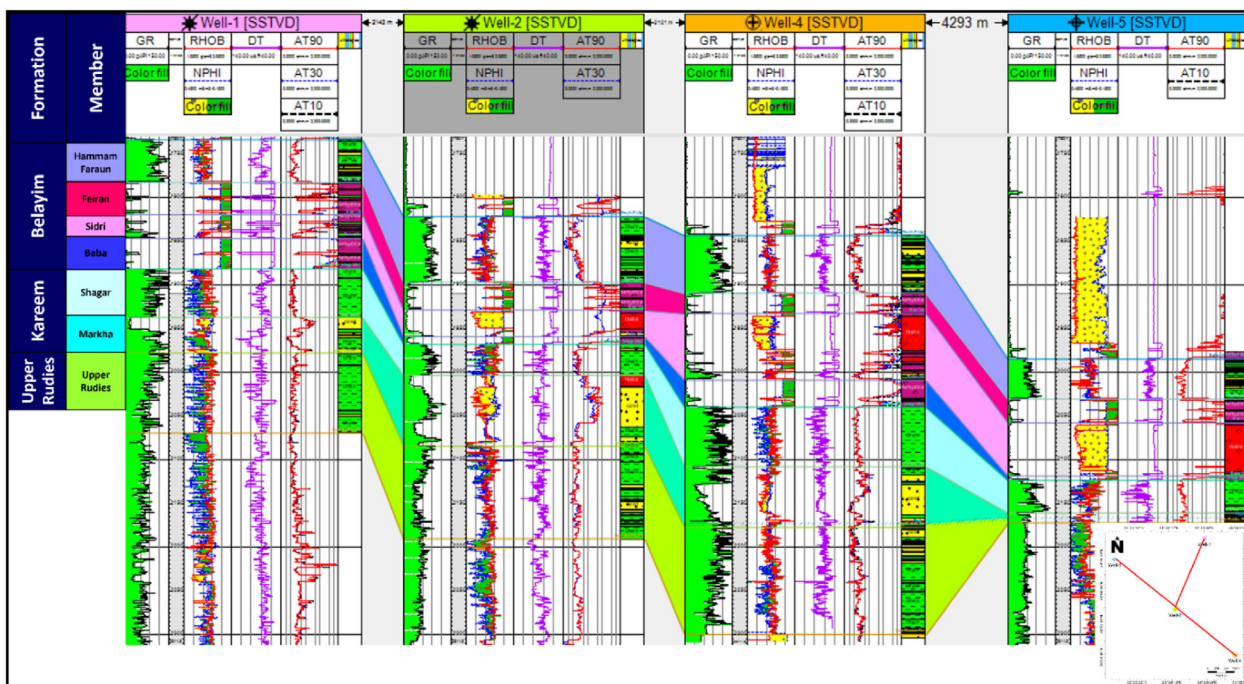


Figure 4. Well correlation showing log responses. The upper zone of Belayim is sand with shale intercalations, and the lower zones are anhydrite with salt and shale. Kareem’s upper zone is mainly shale, while the lower zone is sand with shale intercalations. The upper zone of Upper Rudies is composed of sand and shale intercalations.

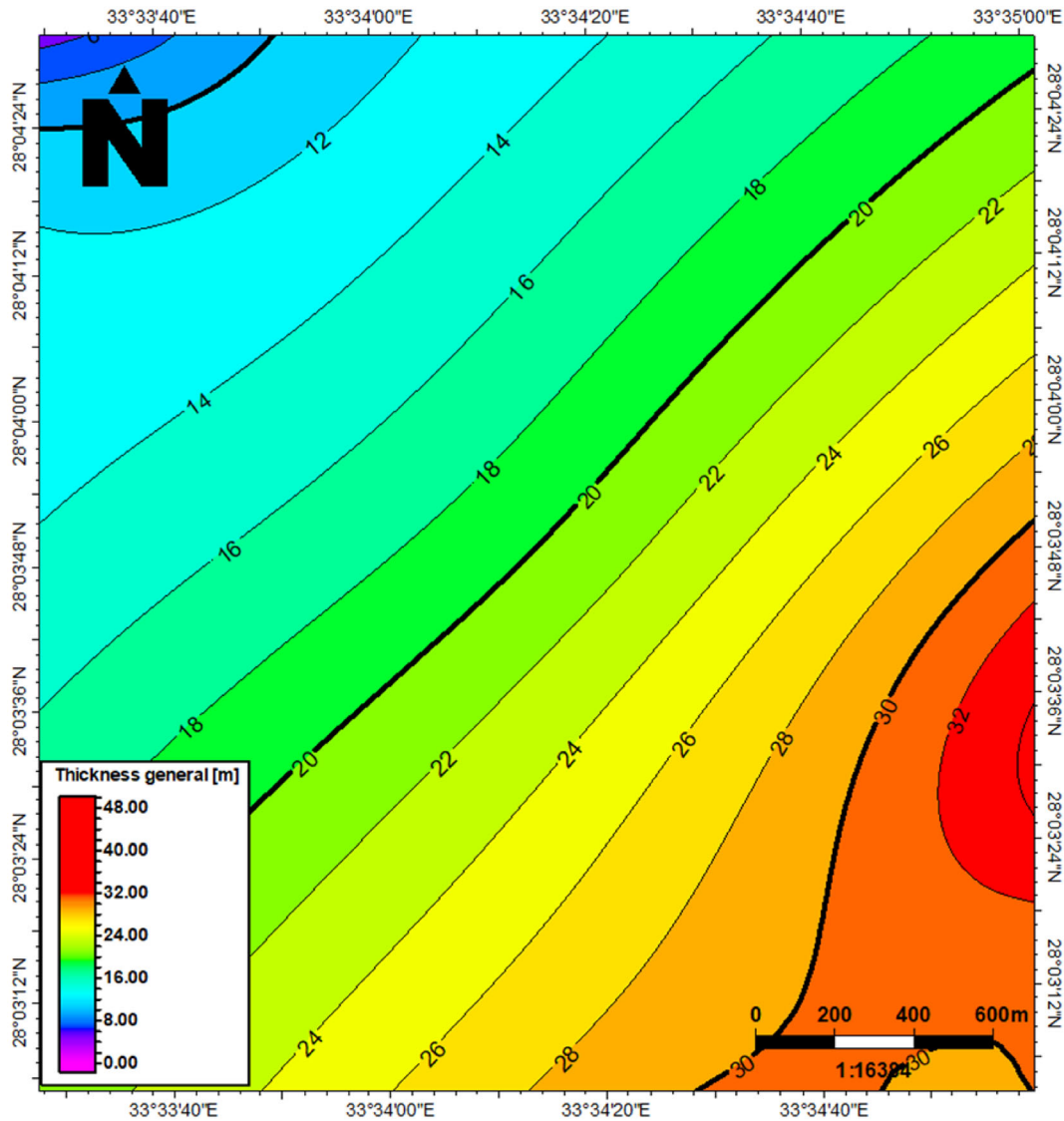


Figure 5. Sand isolith map of net sand of Hammam Faraun Member from all the wells.

Petrophysical Analysis

The logging data were analyzed to estimate the petrophysical parameters of wells. Wireline logging data of neutron, density, resistivity, sonic, and GR were used to estimate total porosity, effective porosity, V_{sh} , S_w , hydrocarbon saturation, gross thickness, and net thickness of the target zone. GR logs were used to differentiate between the shale and non-shale zones then based on the density,

neutron, and sonic logs the lithological type of the non-shale zones were identified.

V_{sh} values distribution exhibits several variations. The Hammam Faraun zone has V_{sh} range of 0.21–0.30, Markha 0.13–0.29, and Upper Rudies 0.29–0.37. These variations may be due to the heterogeneity of the study area. Porosity values exhibit several variations. The Hammam Faraun zone has porosity range of 0.2–0.26, Markha 0.18–0.24, and Upper Rudies 0.20–0.26.

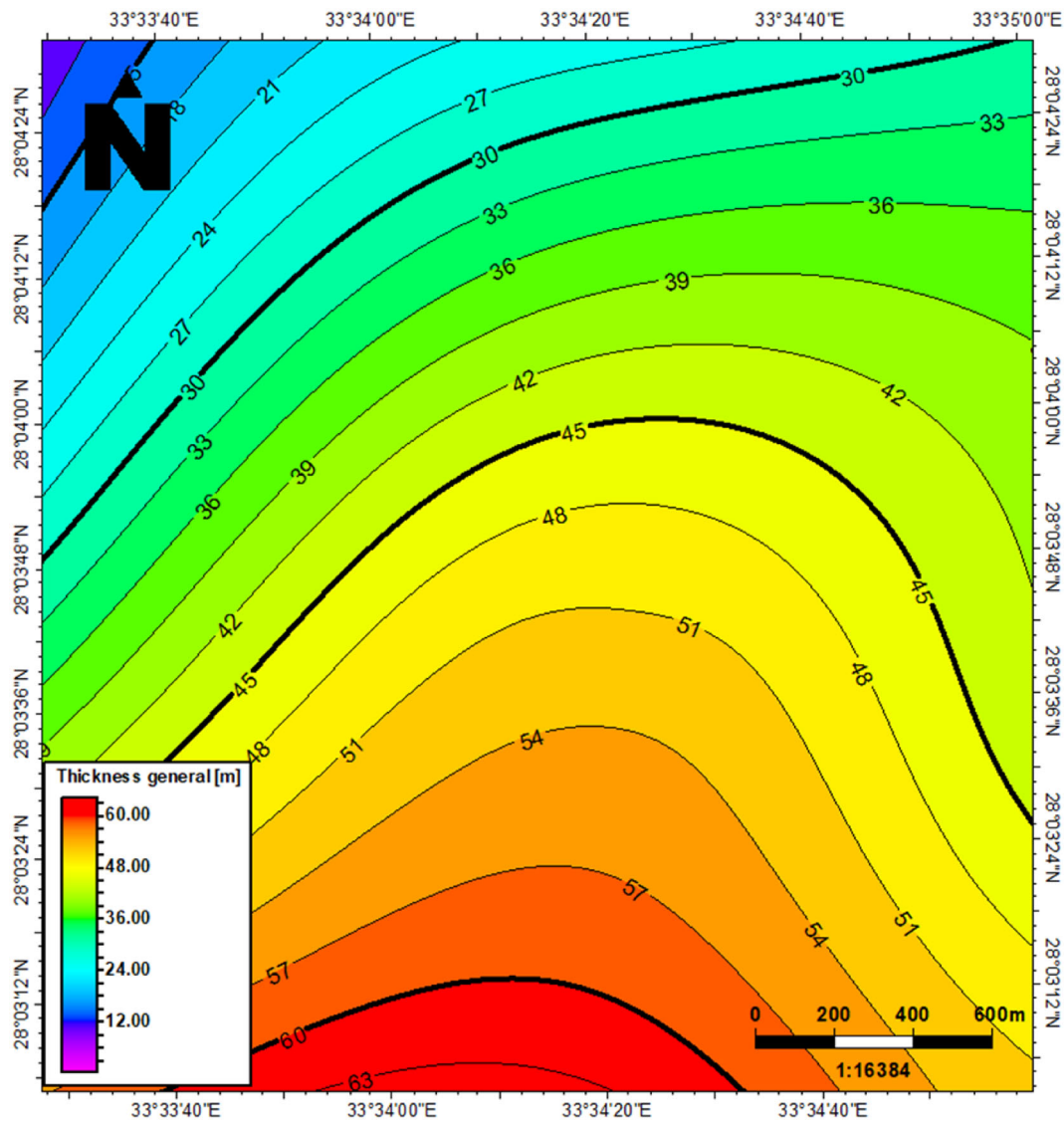


Figure 6. Sand isolith map of net sand of Markha Member from all the wells.

The S_w values distribution exhibits several varieties of increasing and decreasing. The Hammam Faraun zone has S_w ranges of 0.34–0.49, Markha 0.16–0.38, and Upper Rudies 0.35–0.4. These may be due to the heterogeneity of the facies in the study area. Table 1 represents the petrophysical analysis of the Hammam Faraun, Markha, and Upper Rudies reservoirs in the five studied wells. All the obtained petrophysical parameters show good agreement with previous researches (Ata et al., 2012; Ramadan et al., 2019; Farouk et al., 2022).

Seismic Data Interpretation

Faults were interpreted and tracked in all the seismic sections. The interpreted seismic section exhibited a main crest structure bounded by two major faults and affected by minor faults (Fig. 8). All major and minor faults affect the three picked reflectors. The reflector of the Belayim Formation is represented by a peak as the wells have encountered shale after sand, also Kareem and Upper Rudies Formations are marked by peak amplitude for the same reason. The interpreted structures are in

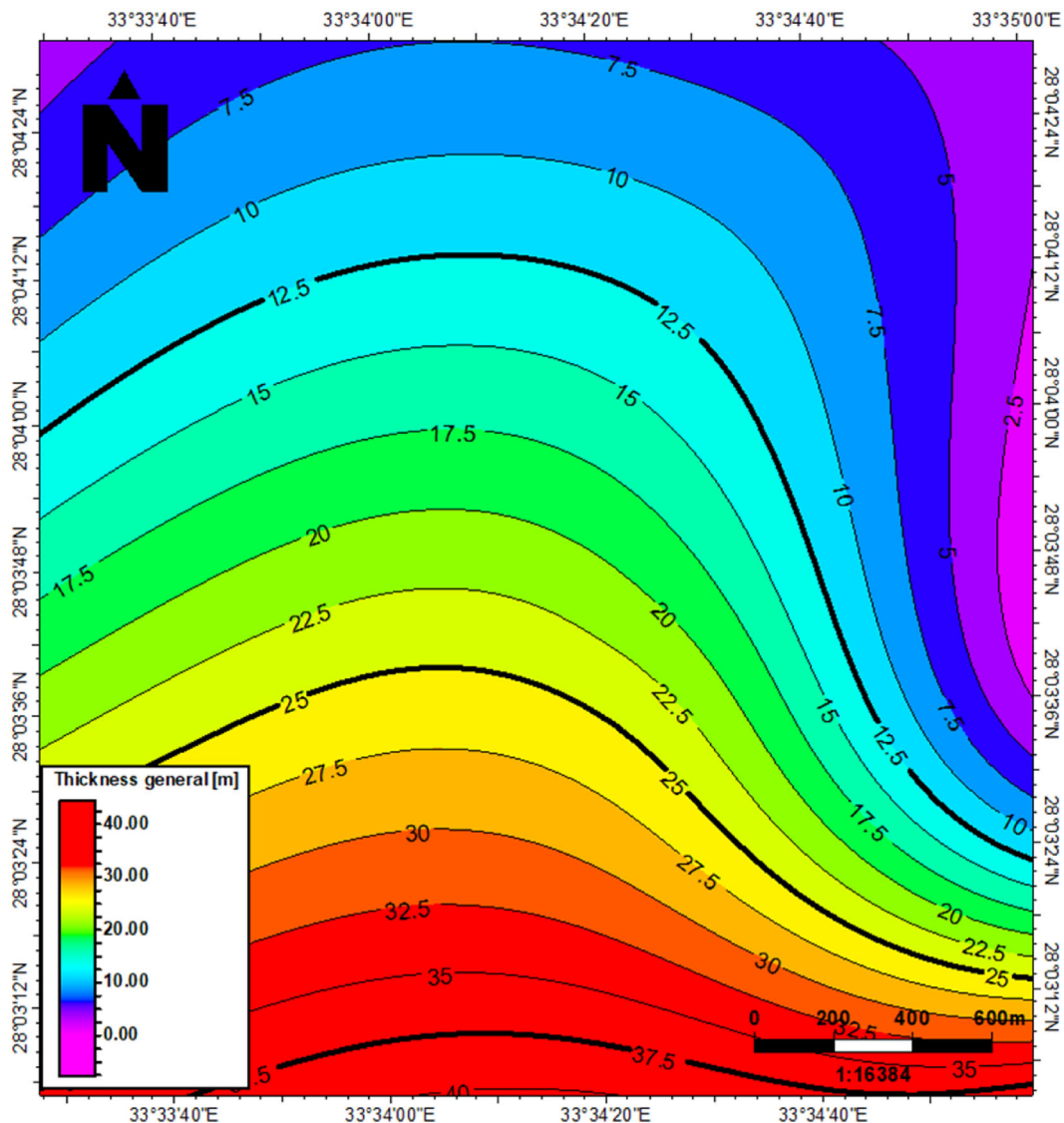


Figure 7. Sand isolith map of net sand of Upper Rudies Member from all the wells.

agreement with previous work (Ata et al., 2012; Okeil et al., 2019)

Depth structure contour maps were created for areas near the Belayim, Kareem, and Rudies Formation tops. The reflectivity of the three formation tops is moderate to low due to the presence of salt. Surfaces were constructed near the top of the three formations. The depth values of the Belayim Formation were in the range of 155–2540 m, the depth values of the Kareem surface map were in the range of 1700–2700 m, and the Rudies surface has a depth range of 1800–2820 m (Figs. 9, 10, and 11, respec-

tively). These depth variations reflect the effect of structural features in the study area.

All the depth structure contour maps showed a main fault block bounded by two major faults extending along the area trending NW–SE. Most of the major faults throwing northeast with large displacement are branched in the northern direction into smaller faults; faults throwing southwest with smaller displacement relative to the northeast fault were noticed (Figs. 9, 10, and 11). All the seismic data and the constructed maps were in the depth domain.

Table 1. Petrophysical analysis of the study area

Parameters	Zone					
	Wells	Well #1	Well #2	Well #3	Well #4	Well #5
Volume of shale (V_{sh}) %	Hammam Faraun	0.21	0.27	0.25	0.31	0.30
	Markha	0.13	0.25	0.28	0.29	0.26
	Upper Rudies	0.34	0.29	0.33	0.37	0.34
Total porosity (phit) %	Hammam Faraun	0.24	0.24	0.26	0.23	0.20
	Markha	0.24	0.18	0.22	0.20	0.24
	Upper Rudies	0.26	0.25	0.26	0.22	0.20
Effective porosity (phie) %	Hammam Faraun	0.17	0.18	0.185	0.17	0.14
	Markha	0.18	0.16	0.15	0.16	0.17
	Upper Rudies	0.19	0.19	0.20	0.16	0.19
Water saturation (S_w) %	Hammam Faraun	0.34	0.35	0.367	0.43	0.49
	Markha	0.24	0.169	0.23	0.38	0.34
	Upper Rudies	0.35	0.40	0.38	0.37	0.35
Hydrocarbon saturation (Sh) %	Hammam Faraun	0.66	0.65	0.64	0.57	0.51
	Markha	0.76	0.84	0.77	0.62	0.66
	Upper Rudies	0.65	0.6	0.62	0.63	0.65
Gross thickness	Hammam Faraun	51	75	68.5	66	46
	Markha	45	81	88	75	10
	Upper Rudies	95	100	15	85	95
Net thickness	Hammam Faraun	15	23	35	34	10
	Markha	25	51	42	48	3
	Upper Rudies	6	21	2.5	33	6

Eight normal faults were picked in the area of study and named $F1$, $F2$, $F3$, $F4$, $F5$, $F6$, $F7$, and $F8$, and they affect the studied stratigraphic units (Fig. 8). The study area is subdivided structurally by the two main bounding faults into three blocks: eastern, western, and central blocks and the central horst block is subdivided into subblocks. According to the study, additional prospect areas can be identified that offer a good location for hydrocarbon accumulation (Fig. 9, 10, 11).

3D Geo-Static Modeling

Structural modeling starts by picking and interpreting geological surfaces (horizons and faults) and then modeling contacts between geological surfaces (e.g., fault and fault, horizon and horizon, fault and horizon) (Euler et al., 1999). The property model exhibits the distribution of the facies and petrophysical parameters (sand to shale ratio, porosity, and fluid distribution) as estimated from petrophysical analysis (Yan-lin et al., 2011). It is important to differentiate and execute an accurate structural model according to geologic information because research in the energy industry (Wu & Xu,

2004) focuses on enhancing subsurface resource utilization via enhanced resource evaluation with production efficiency (Radwan et al., 2022).

A structural model is constructed in three main steps: geometry definition, fault framework modeling, and horizon modeling. Geometry is defined by defining the x-y coverage for the area of interest from the seismic survey automatically. Faults are modeled from interpreted faults in seismic sections in the depth domain. A crucial step in creating a structural model is to accurately represent the fault relationships. Time will be saved later in the workflow if the fault models are accurate and geologically reasoned, faults relationships can be edited (Fig. 12).

Figure 13 represents the fault modeling of the study area. Horizons were modeled using interpreted horizons, thickness maps, and the well-defined tops of the study area (Fig. 13). This model was subdivided into zones (Figs. 18a, 19a). The Belayim Formation is subdivided into four zones (Hammam Faraun, Fieran, Sidri, and Baba), the Kareem Formation into two zones (Markha and Shagar), and the Rudies Formation into two zones (Upper and Lower Rudies). This model was finely layered; the Hammam Faraun Member was subdivided into 25 layers, the Markha Member into 40 layers, and the Rudies

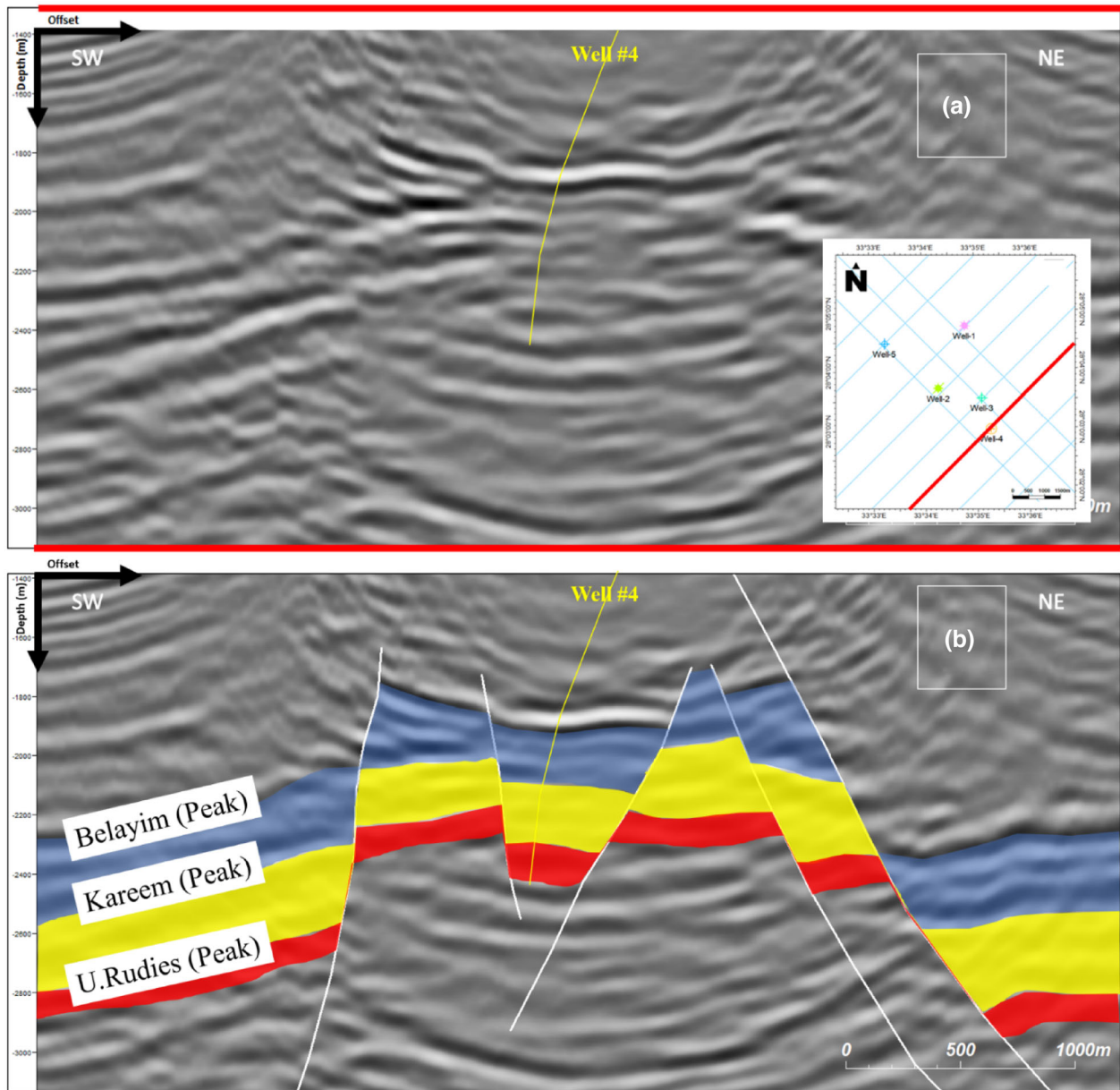


Figure 8. Seismic section from the southern part of Amal area: (a) un-interpreted and (b) interpreted sections showing the extensional faults and horizons of interest.

Member into 60 layers. This model had relatively small xyz cell dimensions to capture important flow units. This model was constructed for three main formations (Belayim, Kareem, and Rudies) in the depth domain about the structural elements (Fig. 13). The structural model showed the main crest structure bounded by two major faults trending

NE–SW. The main horst structure is affected by synthetic and antithetic faults that form small horst and small graben. One of the major faults throws large displacement northeast and it is branched into smaller faults in the northern part of the study area, and the other throws a smaller displacement relative to the northeast fault.

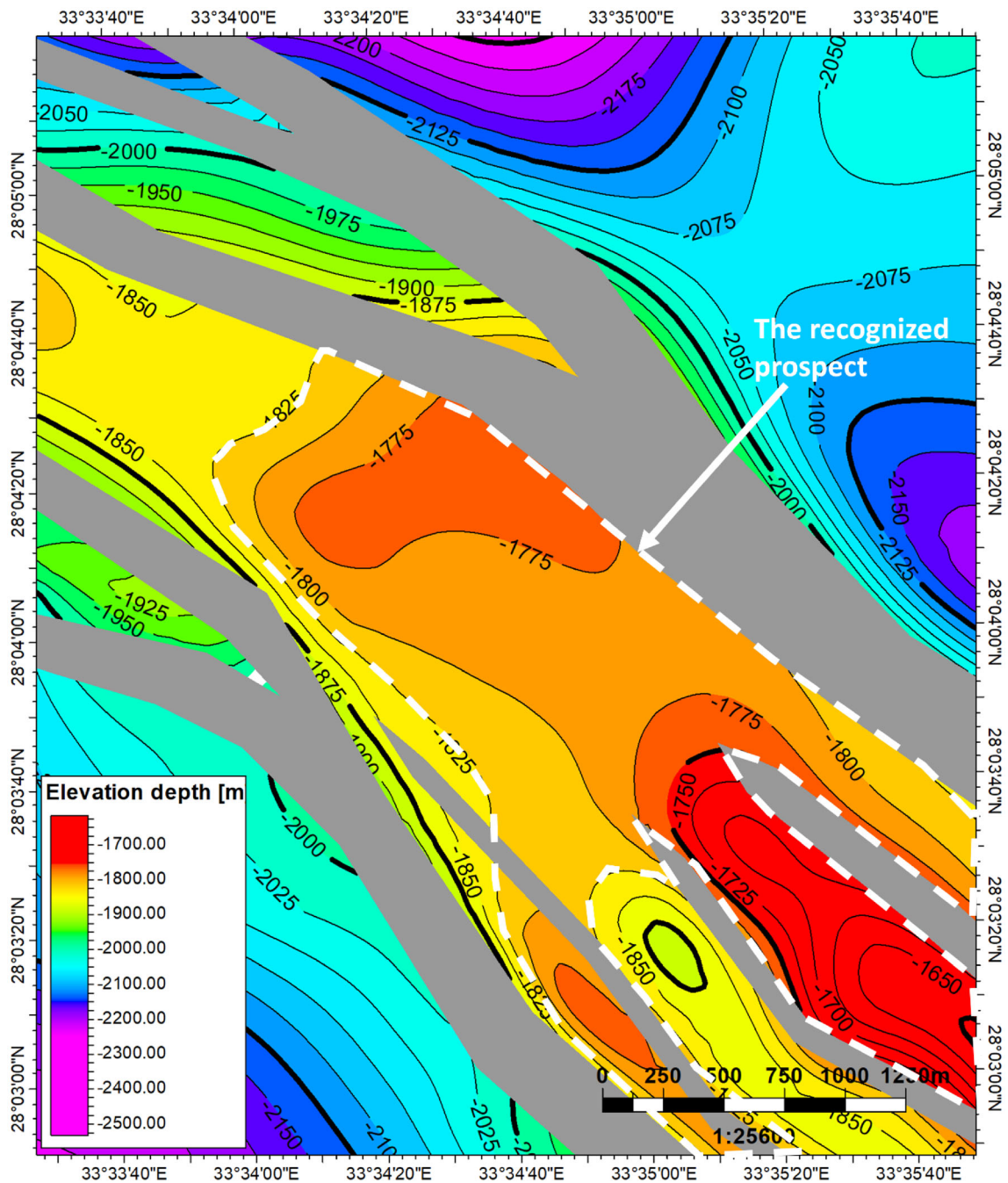


Figure 9. Depth structure contour map of near the top of the Belayim Formation with prospect location highlighted in the white dashed polygon. Grey polygon represents fault heaves.

The property modeling represents the filling process of the cellular grid of the model with specific properties by assigning the well log data to grid cells (scaling up well logs). A single log value will be

generated for each grid cell by averaging all the log values that fall inside that cell using the chosen algorithm. Interpolation methods were used to dis-

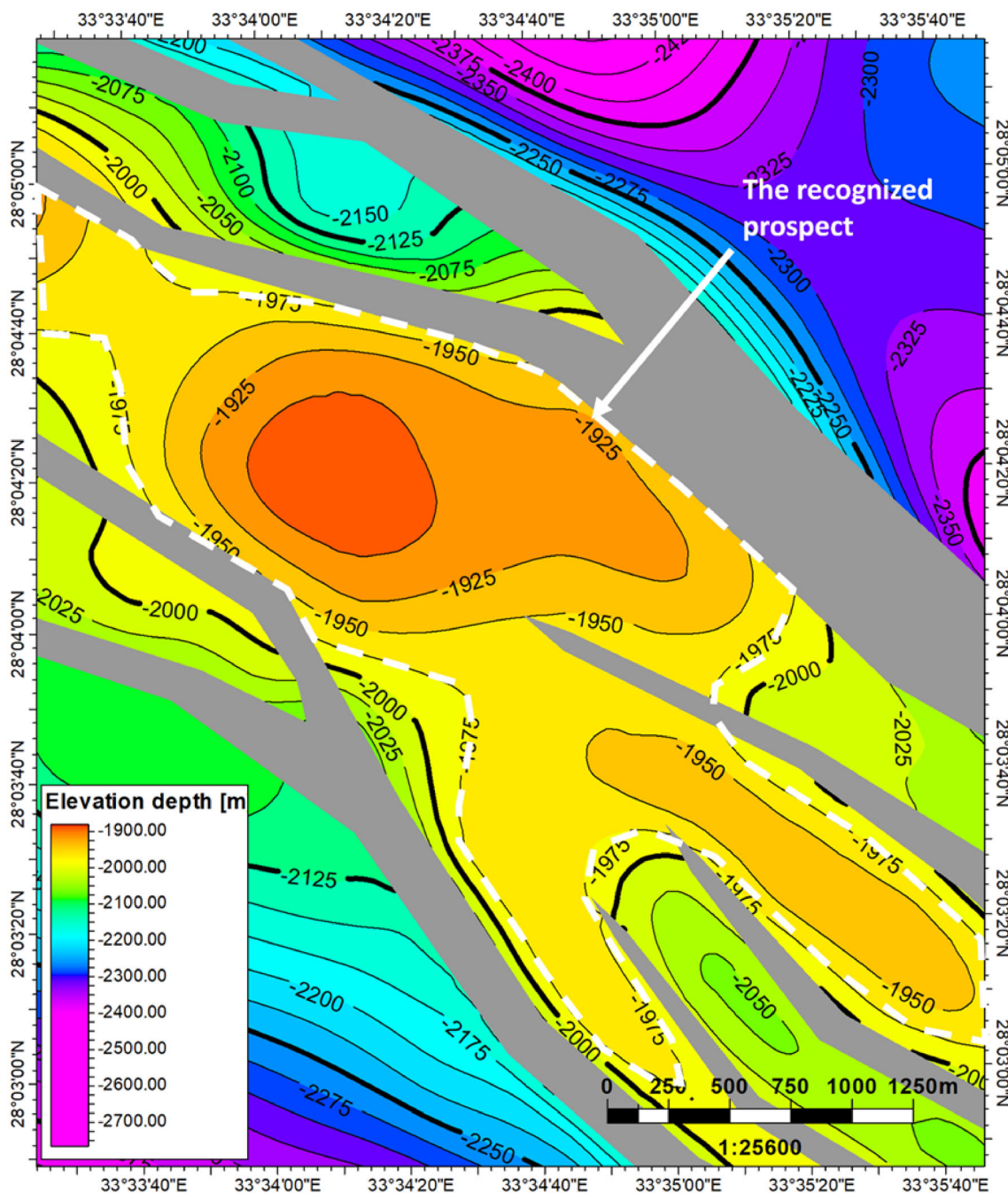


Figure 10. Depth structure contour map near the top of the Kareem Formation with prospect location highlighted in the white dashed polygon. Grey polygons represent fault heaves.

tribute the reservoir properties between and around the wells (Fig. 13).

The facies model was constructed for the Hammam Faraun, Markha, and Upper Rudies

Members using different algorithms to distribute facies randomly. The three main reservoirs are composed mainly of sand and shale. Lithological log curves were constructed based on the wireline logs

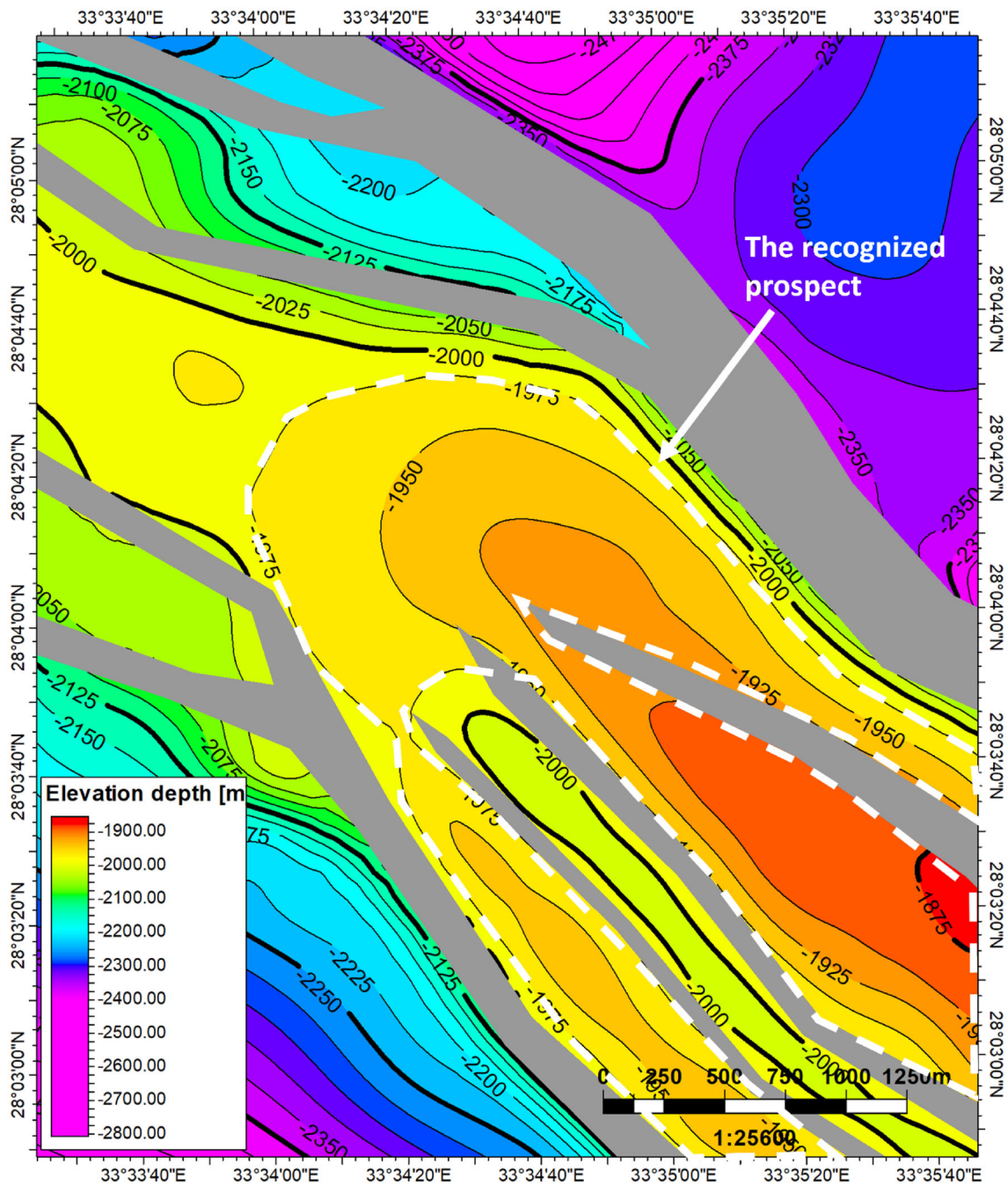


Figure 11. Depth structure contour map of the Rudies Formation with prospect location highlighted in the white dashed polygon. Grey polygons represent fault heaves.

for each well, then scaled up using arithmetic computation, then distributed into geo-cellular grids by the sequential gaussian simulation algorithm method to track sand facies in the three main reservoirs. The

Hamam Faraun exhibits good sandy facies in the northeastern part of the area. The Markha and Upper Rudies exhibit good sandy facies in the cen-

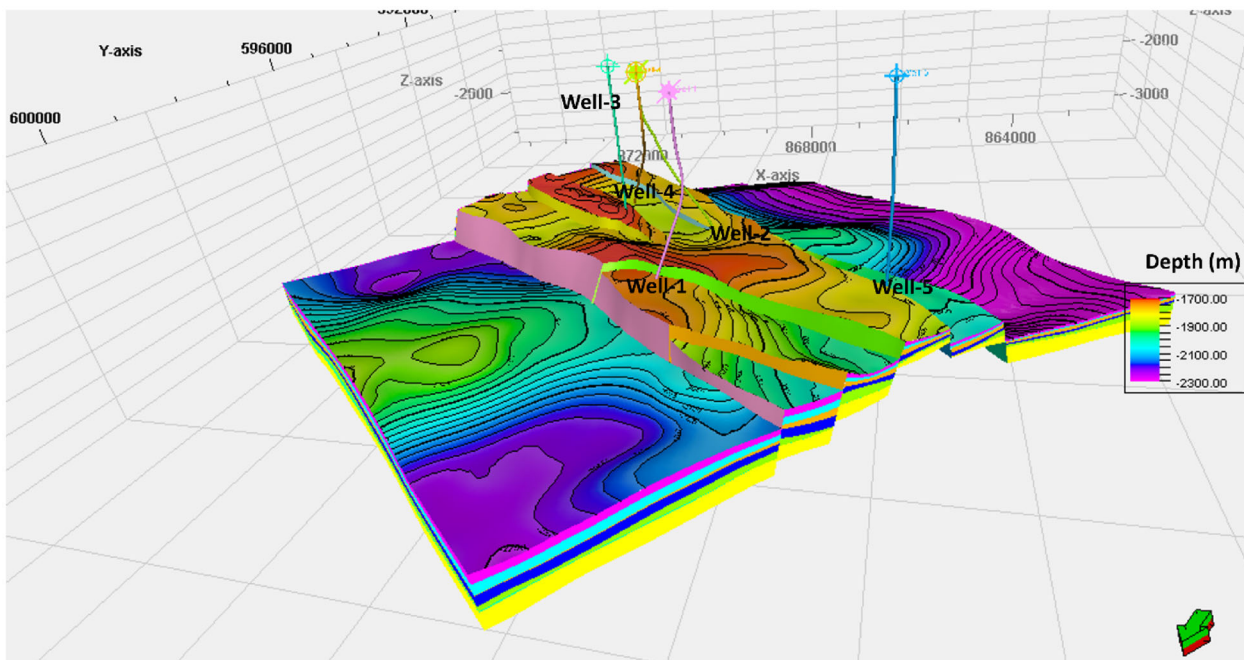


Figure 12. 3D structural model across the study area with zones.

tral part of the area, which is the horst block (Fig. 14a, b).

Figure 14a shows that all the wells encountered the Hammam Faraun zone but with different lithologies. Only very good sandy facies are in well #1, marked by yellow color, compared to the shale facies in the other wells. Figure 14b shows that all the wells encountered the Markha Zone with good sandy facies, marked by yellow areas, except Well #2, which has a shaley facies.

The petrophysical properties modeling for each cell passing through the trajectory of a well can be extracted between the wells in the 3D grid once the log data have been scaled up to the 3D geo-cellular grid. Therefore, each cell in a grid has a value for the selected property. Porosity, V_{sh} and S_w were distributed on the 3D grid using algorithms for the Hammam Faraun Member, the Markha Member, and the Upper Rudies Formation. Porosity models show lateral variations in porosity because of lateral facies change. The Hammam Faraun porosity models show good porosity values in the range of 0.15–

0.23 (Fig. 15a), with porosity increasing toward the central part of the area.

Figure 15a shows that all the wells that encountered the Hammam Faraun zone have very good porosity values, marked by red and yellow areas. The Markha porosity model shows that the porosity increases toward the southwestern part of the area, with values in the range of 0.15–0.22 (Fig. 15b). Figure 15b shows that all the wells that encountered the Markha zone have varieties in the porosity values, which are good at Well #2, Well #3, and Well #4 marked by red to green areas compared to well #1 and Well #5, which have low porosity values marked by blue color. Figures 18a and 19a represent structural traps in the area. All these models were used to evaluate reservoir properties in the area. Figures 18c and 19c exhibit the porosity distribution.

The V_{sh} was calculated using GR logs for the Hammam Faraun, Markha, and Upper Rudies zones. V_{sh} log curves were scaled up using arithmetic computation. The sequential Gaussian simulation algorithm method was used to distribute V_{sh} among

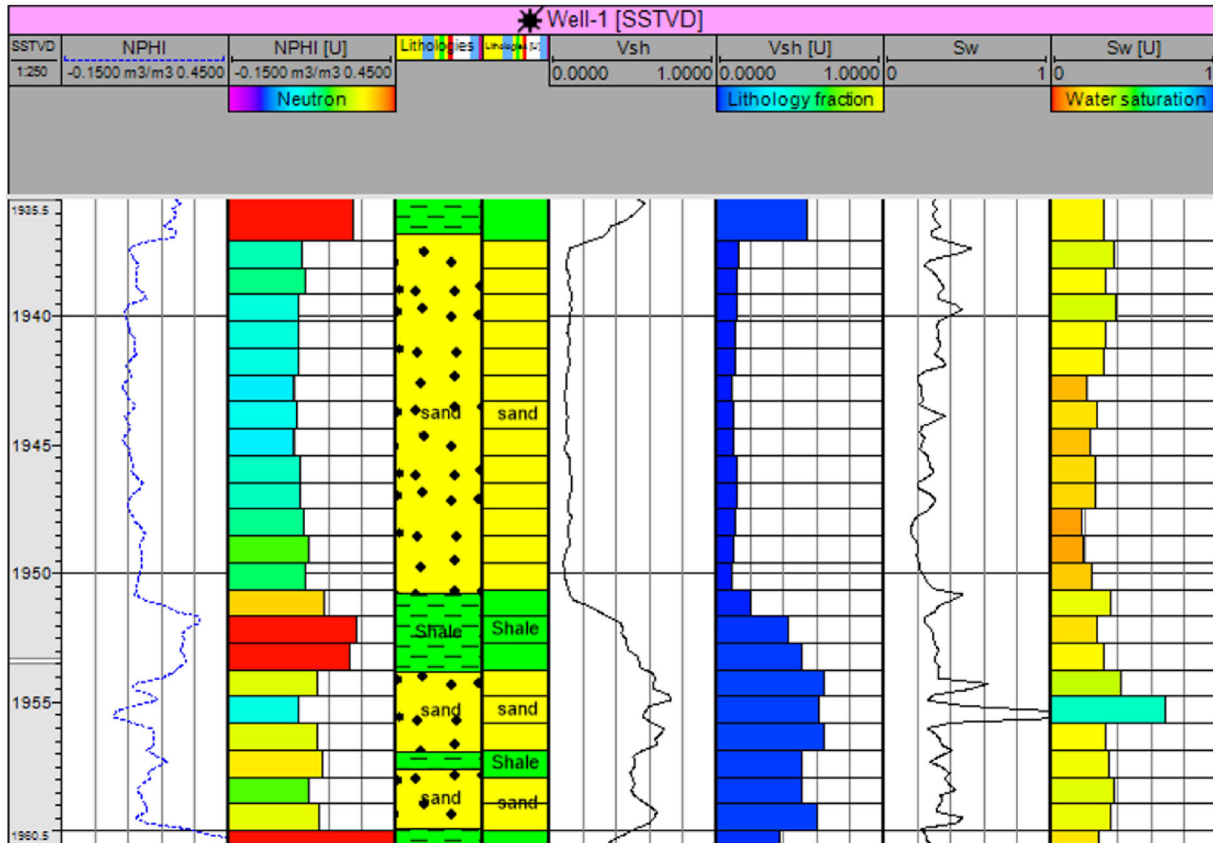


Figure 13. Well #1 logs scale-up.

and around the wells. The V_{sh} models exhibited several variations (Fig. 16a, b). In the Hammam Faraun zone, V_{sh} ranged 0.21–0.31, explained as 0.21 in Well #1, 0.27 in Well #2, 0.25 in Well #3, 0.31 in Well #4, and 0.3 in Well #5. In the Markha zone, V_{sh} ranged 0.13–0.29, explained as 0.13 in Well #1, 0.25 in Well #2, 0.28 in Well #3, 0.29 in Well #4, and 0.26 in Well #5. In the Upper Rudies zone, V_{sh} ranged 0.29–0.37, explained as 0.34 in Well #1, 0.29 in Well #2, 0.33 in Well #3, 0.37 in Well #4, and 0.34 in Well #5. These variations may be due to the heterogeneity of facies of the study area. Figures 18b and 19b represent the structural cross section with V_{sh} distribution of the study area.

The S_w was calculated for Hammam Faraun, Markha, and Upper Rudies zones using the Indonesian formula (Eq. 1) because of shale presence. Using the arithmetic computation, the S_w log was scaled up into the geo-cellular grid of the model.

The sequential Gaussian simulation algorithm method was used to populate water saturation among and around the wells. The S_w models exhibited several varieties from increasing and decreasing (Fig. 17a, b). The Hammam Faraun zone has S_w range of 0.34–0.49, Markha 0.16–0.38, and Upper Rudies 0.35–0.4. These may be due to the heterogeneity of facies of the study area. Figures 18d and 19d represent the structural cross section with S_w distribution of the study area.

Modeling Uncertainties and Quality Control

Modeling is impacted by interpretation uncertainties. Due to limited data availability, poor data quality, difficulties of the reservoir design in estimating flow in a particular reservoir, and modeling process errors, reservoir modeling is commonly

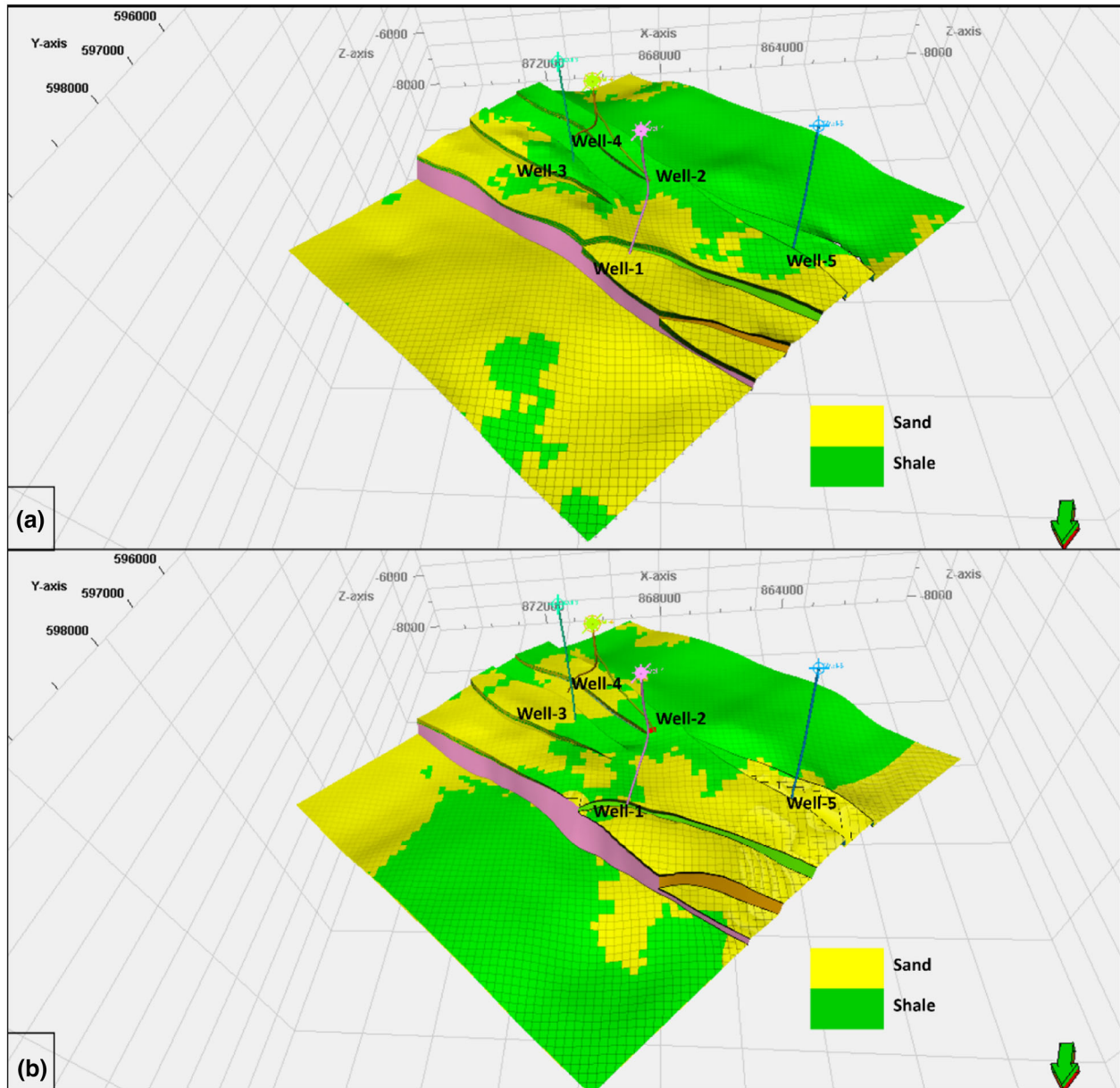


Figure 14. (a) Facies modeling for the Hammam Faraun zone showing sandy facies in well #1 marked by yellow color compared to the shaly facies in the other wells. (b) Facies modeling for the Markha zone showing that all the wells encountered sandy facies marked by yellow areas except Well #2.

plagued by uncertainty (Radwan, 2022). Therefore, it is crucial to assess the input data for quality, quantity, and complexity at different scales, as well as to review fundamental assumptions about the suitability of a modeling workflow in the context of

static reservoir uncertainty. We made an effort to carry out precise interpretations and extract the best-fit input parameters in this work.

To fill up the gaps, general geologic knowledge, local geology, and some prior work experience from

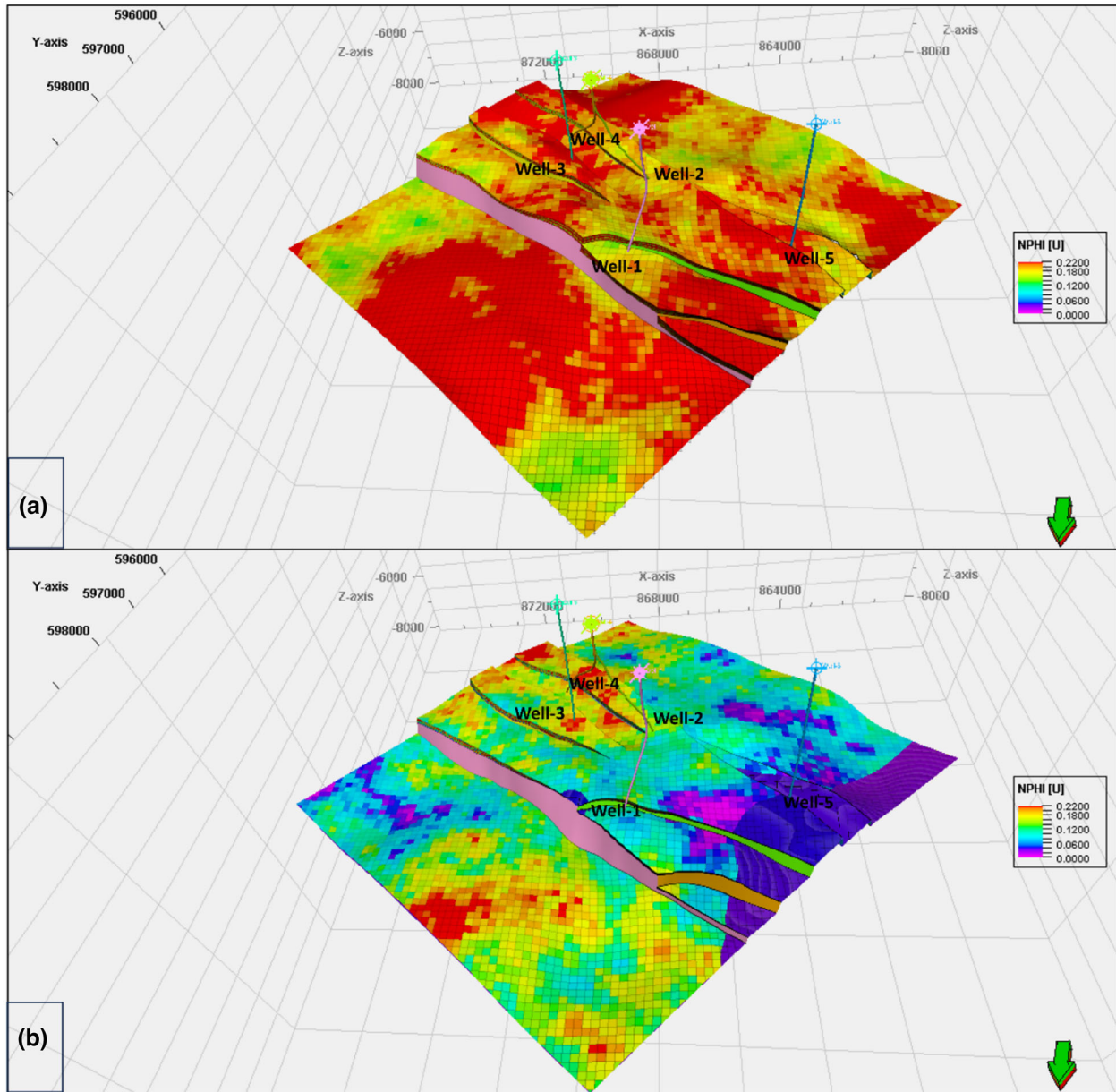


Figure 15. Porosity models of (a) the Hammam Faraun zone and (b) the Markha zone.

nearby oilfields were utilized. As well, we applied several tests to do a quality control check on the resulting model, including the following:

- No negative cells or bulk volumes
- Avoid non-orthogonal cells, as they should always be greater than 45 degrees.
- Avoid having twisted cells that are always close to faults.
- Observe good match between the scaled-up logs and the electrical well logs (Fig. 13).
- Review a reasonable facies distribution.

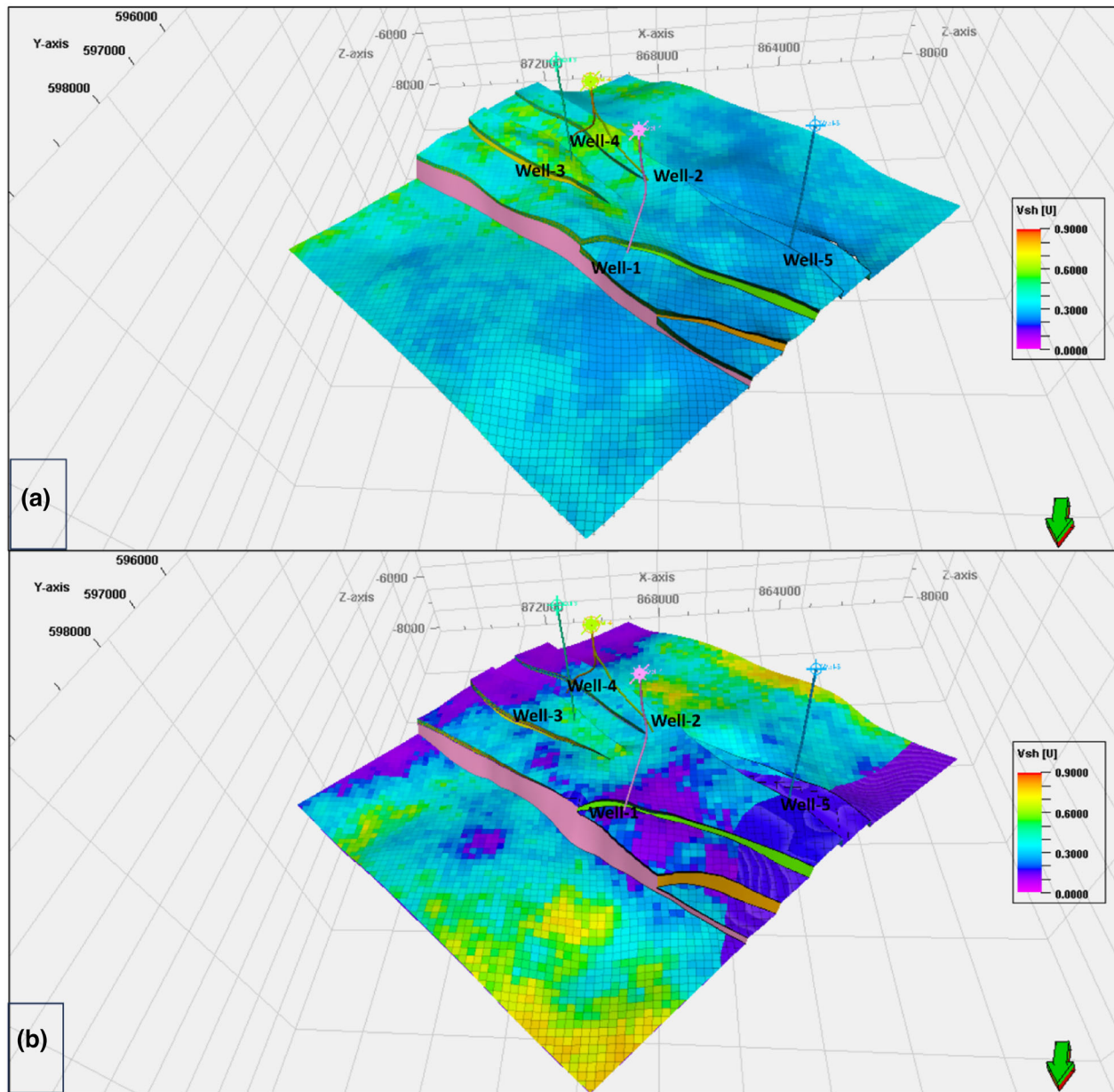


Figure 16. V_{sh} model of (a) the Hammam Faraun zone and (b) the Markha zone.

The main sources of uncertainty in lithofacies modeling are constrained data and reservoir geological information. Therefore, there is a great deal of uncertainty in the 3D structural system's facies or flow unit distribution. In this study, we employed integrated facies analysis and well-log interpretation across the examined wells to try and reduce uncertainty in the facies model.

Prospect Estimation and Reserve Estimation

Prospects are subsurface locations composed of traps, cap rock, reservoir rock, and source rock that can expel hydrocarbon into the trap where the economic conditions are suitable for drilling new wells. Prospects have the potential to produce hydrocarbons but need to be proven (Gluyas and

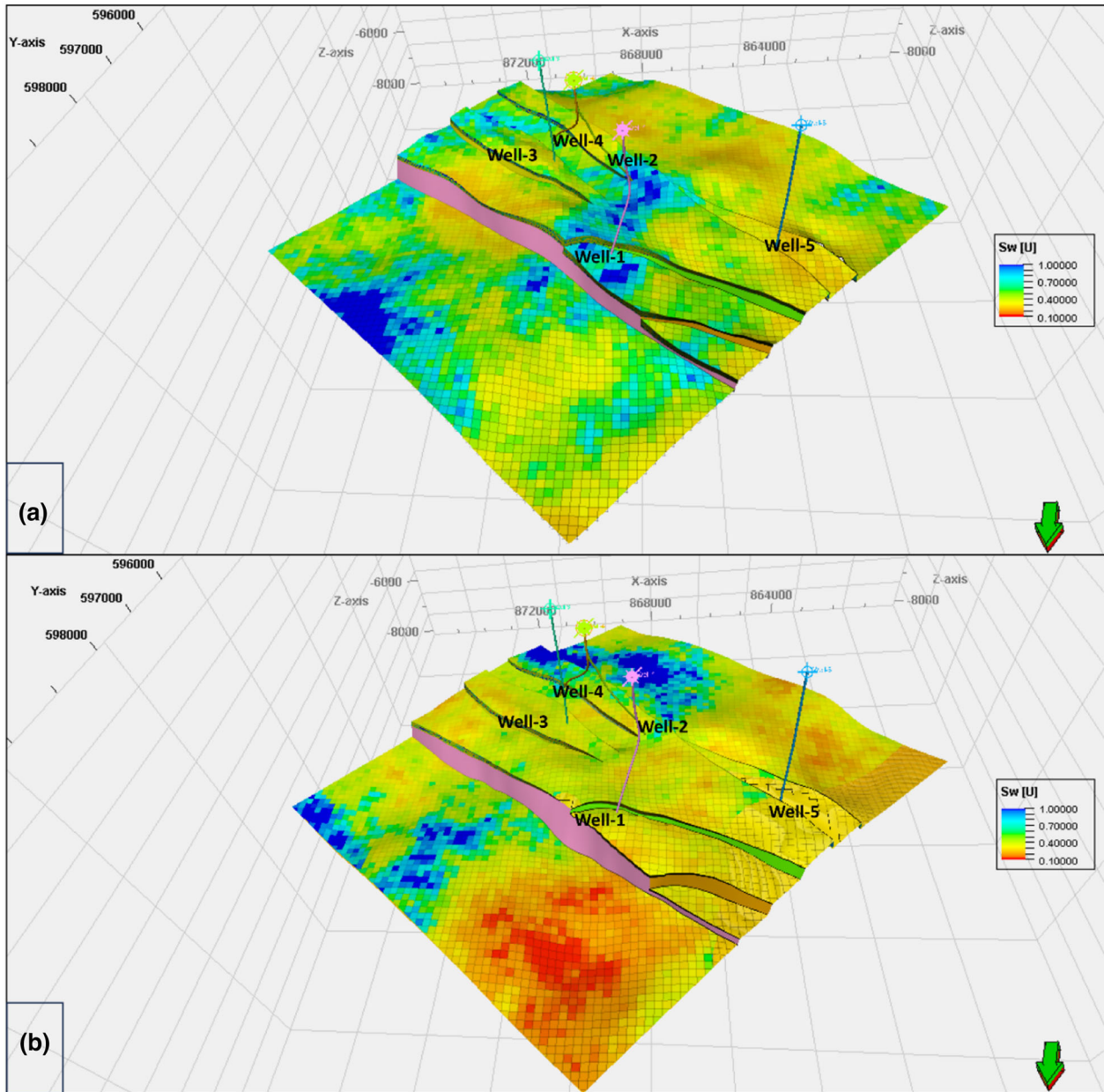
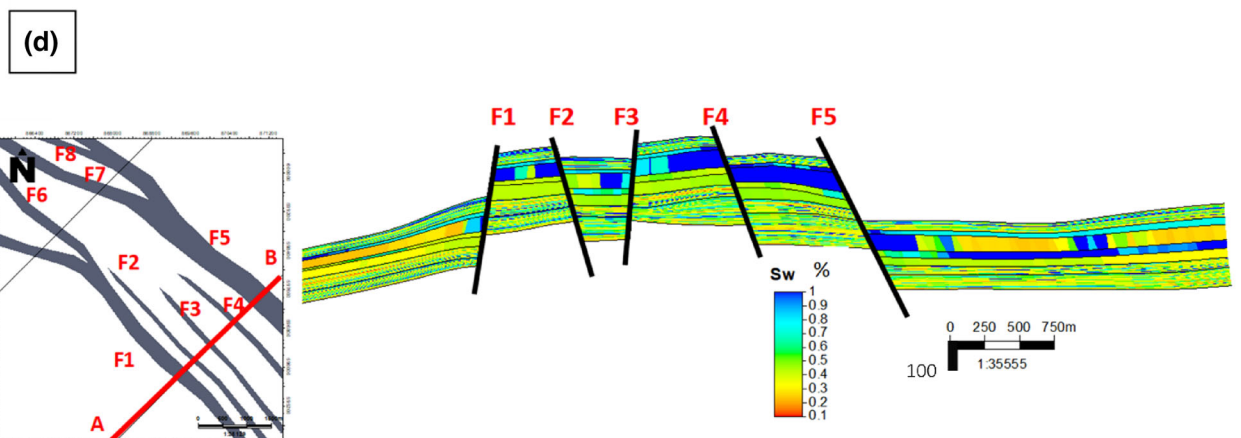
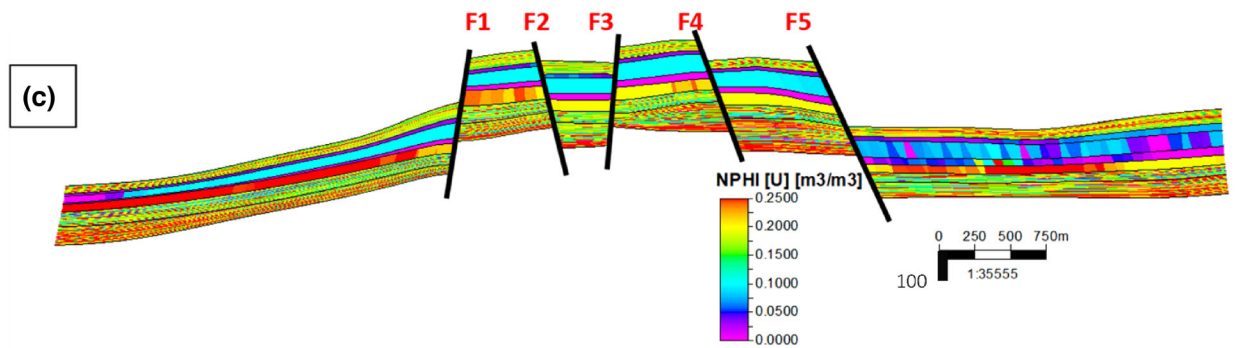
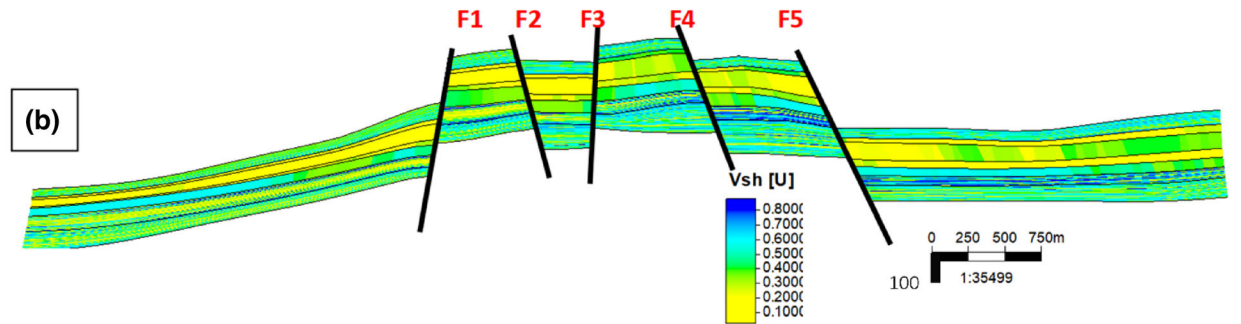
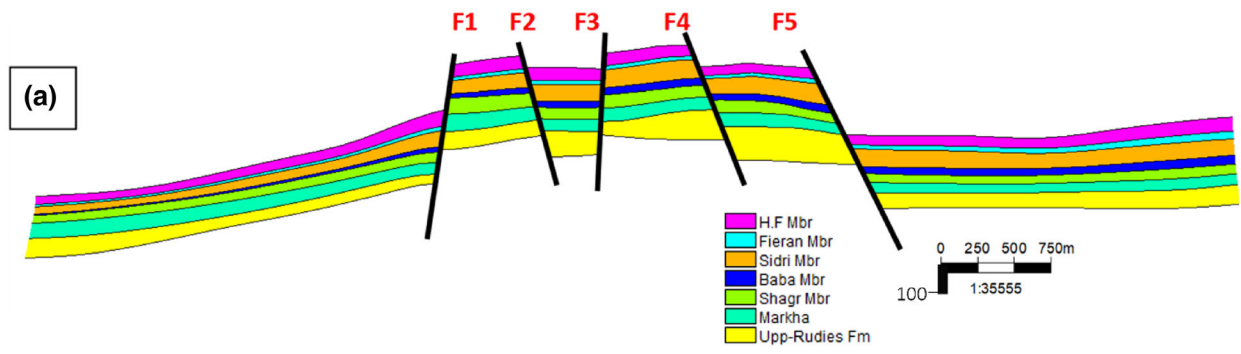


Figure 17. Water saturation model (a) of Hammam Faraun zone and (b) Markha zone.

Swarbrick, 2004). The main objective of reservoir modeling in this study was to evaluate the distribution of facies and locate new prospect locations and drillable positions. Based on the structural contour

maps and the constructed models, the prospect locations were determined depending on their structural closures, seismic interpretation, facies distribution, and petrophysical parameters (Figs. 9,



◀ **Figure 18.** NE-SW integrated A-B Cross section through all formations. (a) Structural cross section with zones. (b) Structural cross section with shale content (V_{sh}). (c) Structural cross section with porosity (NPHI). (d) Structural cross section with S_w .

10, 11). Table 2 shows the deterministic reserve estimations of the three main reservoirs in the southern Gulf of Suez. The volumetric technique was used to estimate the original oil in place based on the following equation:

$$N(t) = \frac{V_b \phi(P(t))(1 - S_w(t))}{Bo(P(t))} \quad (5)$$

where $N(t)$ is original oil in place (STB, stock tank barrel) at time t ; $V_b = 7758 Ah$ is bulk reservoir volume (bbl, barrels), where 7758 is bbl/acre-ft, A is area (acres¹), h is reservoir thickness (ft²); $\Phi(p(t))$ is porosity at reservoir pressure p at time t ; $S_w(t)$ is water saturation at time t ; $Bo(p(t))$ is oil formation volume factor (bbl/STB³) at reservoir pressure p ; $P(t)$ is reservoir pressure (psia) at time t .

CONCLUSIONS

The main focus of the current study was on the interpretation of geological and geophysical data to assess the structure, lithofacies, and petrophysical characteristics of Middle Miocene reservoirs in the southern Gulf of Suez province, as well as their 3D distribution. To estimate the distribution and quality of the intricate Middle Miocene reservoirs and to lessen uncertainty during oilfield development in the research area, we employed integrated datasets in this work. The modeling procedures applied in this work can be used to understand similar reservoirs. The primary results of this investigation were as follows:

- The structural models shows that the area was affected by normal faults trending NW–SE with

downthrown side directed to the southwest and northeast, forming step, horst, and graben rotated fault blocks that provide good structural traps, which can hold good amounts of hydrocarbon.

- The study area’s structural framework is a big compartmentalized horst block.
- The depth values of the Belayim Formation range 155–2540 m, those of the Kareem 1700–2700 m, and those of Rudies 1800–2820 m.
- The sand thickness of the Hammam Faraun Member ranges from null to 50 m, that of Markha Member null to 60 m, and that of Upper Rudies null to 45 m.
- Property and facies modeling showed that the central part of the area is a potential area with good reservoir properties.
- The modeling results of the study area show that the Hammam Faraun zone is a good reservoir, with porosity values ranging 0.15–0.23, the porosity increasing toward the central part of the area, V_{sh} ranging 0.21–0.31, S_w ranging 0.34–0.49, net pay thickness ranging 10–35 m, and sandy facies increasing toward the northeastern part of the area according to the facies model.
- The Markha zone also is a good reservoir, with porosity increasing toward the southeastern part of the area with values ranging 0.15–0.22, V_{sh} ranging 0.13–0.29, S_w ranging 0.16–0.38, net pay thickness ranging 3–51 m, and very good sandy facies at the horst block, which is the central part of the area.
- The Upper Rudies exhibit good reservoir properties with porosity values ranging 0.16–0.23, V_{sh} ranging 0.29–0.37, S_w ranging 0.35–0.4, net pay thickness ranging 3–33 m, and good sandy facies at the central part of the area.
- We merged numerous datasets to improve the modeling of the complex Middle Miocene reservoirs and lower the typical uncertainties related to the static modeling procedure.

¹ 1 acres = 4046.85 m²

² 1 ft = 0.3048 m

³ 1 bbl/STB = 0.159 m³

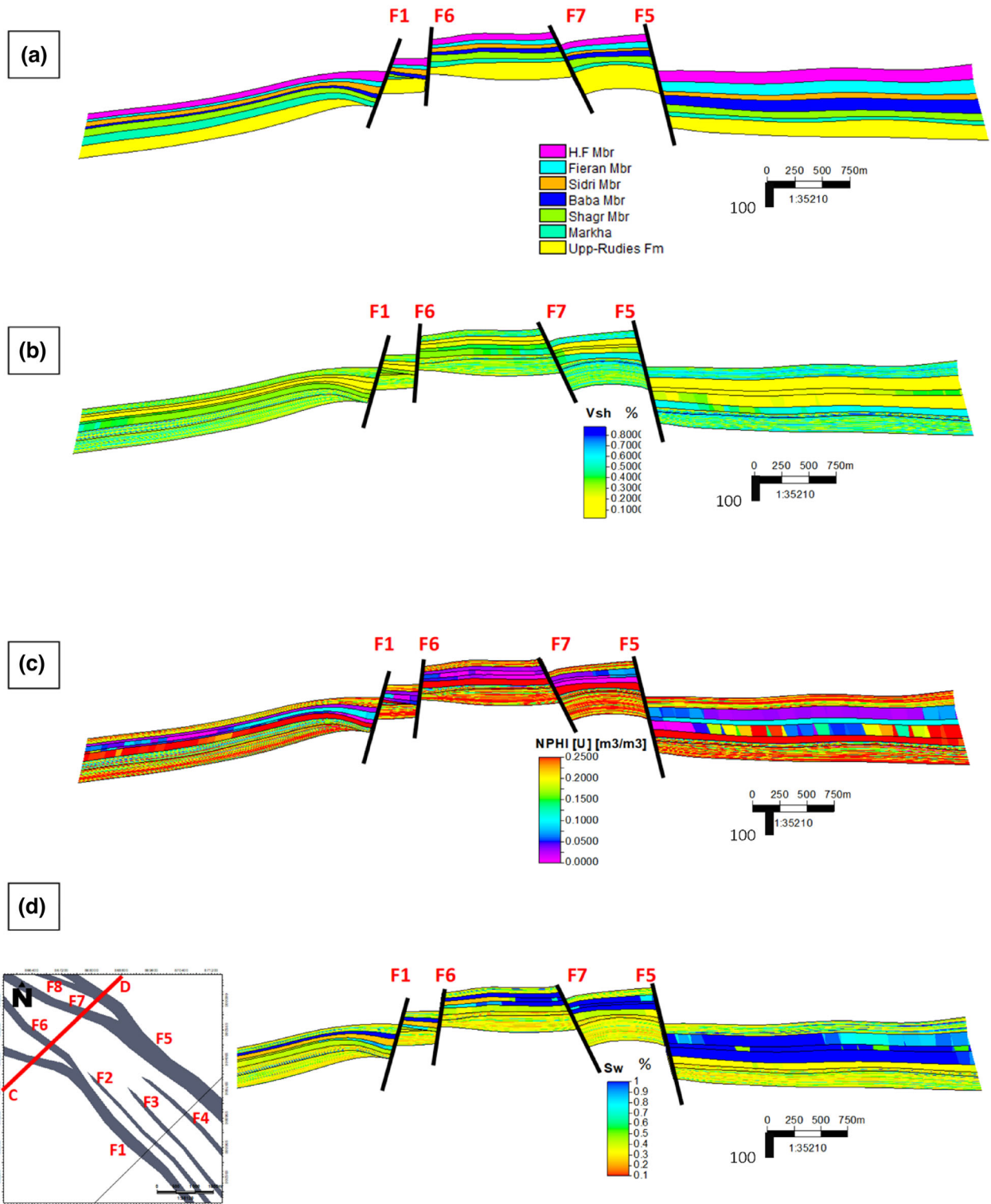


Figure 19. NE-SW integrated C-D Cross section through all formations. (a) Structural cross section with zones. (b) Structural cross section with shale content (V_{sh}). (c) Structural cross section with porosity (NPHI). (d) Structural cross section with S_w .

Table 2. Deterministic reserve estimates for the identified prospects of the Hammam Faraun, Markha, and Upper Rudies reservoirs

Prospects	STOIP (MMSTB)	Reserves (MMSTB)
Hammam Faraun	4922	1723
Markha	13,682	4758
Upper Rudies	141	50

STOIP, stands for stock tank oil initially in place; MMSTB, stands for million stock tank barrels (1 MMSTB = 158987.29493 m³).

- We highly recommend drilling more development wells in the determined prospects.

ACKNOWLEDGMENT

The authors would like to acknowledge the Egyptian General Petroleum Cooperation for providing the data and Cairo University's faculty of science and geophysics department for providing all the necessary resources to accomplish this work.

FUNDING

Open access funding provided by The Science, Technology & Innovation Funding Authority (STDF) in cooperation with The Egyptian Knowledge Bank (EKB).

DATA AVAILABILITY

Data are however available from authors upon reasonable and with permission of The Egyptian General Petroleum Cooperations.

DECLARATIONS

Conflict of Interests No financial and non-financial competing interests.

OPEN ACCESS

This article is licensed under a Creative Commons Attribution 4.0 International License, which permits use, sharing, adaptation, distribution and reproduction in any medium or format, as long as you give appropriate credit to the original

author(s) and the source, provide a link to the Creative Commons licence, and indicate if changes were made. The images or other third party material in this article are included in the article's Creative Commons licence, unless indicated otherwise in a credit line to the material. If material is not included in the article's Creative Commons licence and your intended use is not permitted by statutory regulation or exceeds the permitted use, you will need to obtain permission directly from the copyright holder. To view a copy of this licence, visit <http://creativecommons.org/licenses/by/4.0/>.

REFERENCES

- Abdel-Fattah, M., Dominik, W., Shendi, E., Gadallah, M., & Rashed, M. (2010). 3D integrated reservoir modeling for upper safa gas development in Obaiyed field, Western Desert, Egypt. In *72nd EAGE conference and exhibition incorporating SPE EUROPEC 2010* (pp. cp-161).
- Abdelmaksoud, A., Amin, A. T., El-Habaak, G. H., & Ewida, H. F. (2019a). Facies and petrophysical modeling of the Upper Bahariya Member in Abu Gharadig oil and gas field, North Western Desert, Egypt. *Journal of African Earth Sciences*, *149*, 503–516.
- Abdel-Fattah, M. I., Metwalli, F. I., & El Sayed, I. M. (2018). Static reservoir modeling of the Bahariya reservoirs for the oilfields development in South Umbarka area, Western Desert, Egypt. *Journal of African Earth Sciences*, *138*, 1–13.
- Abdelmaksoud, A., Ewida, H. F., El-Habaak, G. H., & Amin, A. T. (2019b). 3D structural modeling of the Upper Bahariya Member in Abu Gharadig oil and gas field, North Western Desert, Egypt. *Journal of African Earth Sciences*, *150*, 685–700.
- Abdelmaksoud, A., & Radwan, A. A. (2022). Integrating 3D seismic interpretation, well log analysis, and static modeling for characterizing the Late Miocene reservoir, Ngatoro area, New Zealand. *Geomechanics and Geophysics for Geo-Engineering and Geo-Resources*, *8*(2), 63.
- Abuzaid, M., Metwally, A., Mabrouk, W., Khalil, M., & Bakr, A. (2019). Seismic interpretation for the Jurassic/Paleozoic reservoirs of QASR gas field, Shushan-Matrouh basin northwestern Desert, Egypt. *Egyptian Journal of Petroleum*, *28*(1), 103–110.
- Afifi, A. S., Moustafa, A. R., & Helmy, H. M. (2016). Fault block rotation and footwall erosion in the southern Suez rift: Implications for hydrocarbon exploration. *Marine and Petroleum Geology*, *76*, 377–396.
- Alsharhan, A. S. (2003). Petroleum geology and potential hydrocarbon plays in the Gulf of Suez rift basin, Egypt. *AAPG Bulletin*, *87*(1), 143–180.
- Asquith, G. B., & Gibson, C. R. (1982). *Basic well log analysis for geologists* (Vol. 3). American Association of Petroleum Geologists.
- Ata, A. S. A., Azzam, S. S., & El-Sayed, N. A. (2012). The improvements of three-dimensional seismic interpretation in comparison with the two-dimensional seismic interpretation in Al-Amal oil field, Gulf of Suez, Egypt. *Egyptian Journal of Petroleum*, *21*(1), 61–69.
- Attia, M. M., Abudeif, A. M., & Radwan, A. E. (2015). Petrophysical analysis and hydrocarbon potentialities of the un-

- tested Middle Miocene Sidri and Baba sandstone of Belayim Formation, Badri field, Gulf of Suez, Egypt. *Journal of African Earth Sciences*, 109, 120–130.
- Avseth, P., Mukerji, T., Mavko, G., & Dvorkin, J. (2010). Rock-physics diagnostics of depositional texture, diagenetic alterations, and reservoir heterogeneity in high-porosity siliciclastic sediments and rocks—A review of selected models and suggested workflows. *Geophysics*, 75(5), 75A31–75A47.
- Bilodeau, B., De, G., Wild, T., Zhou, Q., & Wu, H. (2002). Integrating formation evaluation into earth modeling and 3-D petrophysics. In *SPWLA 43rd annual logging symposium*. OnePetro.
- Bosworth, W., Huchon, P., & McClay, K. (2005). The red sea and Gulf of Aden basins. *Journal of African Earth Sciences*, 43(1–3), 334–378.
- Bosworth, W., & McClay, K. (2001). Structural and stratigraphic evolution of the Gulf of Suez rift, Egypt: A synthesis. *Mémoires du Muséum national d'histoire naturelle*, 1993(186), 567–606.
- Bryant, I. D., & Flint, S. S. (1992). Quantitative elastic reservoir geological modeling: problems and perspectives. *The Geological Modeling of Hydrocarbon Reservoirs and Outcrop Analogues*, 8, 1–20.
- Coleman, R. G. (1993). *Geological evolution of the Red Sea* (p. 186). Oxford University Press.
- Colletta, B., Le Quellec, P., Letouzey, J., & Moretti, I. (1988). Longitudinal evolution of the Suez Rift Structure (Egypt). *Tectonophysics*, 153, 221–233.
- Cosentino, L. (2005). Static reservoir study. *Encyclopaedia of Hydrocarbons*, 1, 553–573.
- Cressie, N. (1990). The origins of kriging. *Mathematical Geology*, 22, 239–252.
- De Jager, G., & Pols, R. W. J. (2006). A fresh look at integrated reservoir modeling software. *First Break*, 24, 10.
- Euler, N., Sword Jr, C. H., & Dulac, J. C. (1999). Editing and rapidly updating a 3d earth model. In *SEG technical program expanded abstracts 1999* (pp. 950–953). Society of Exploration Geophysicists.
- Fagin, S. W. (1991). Seismic modeling of geologic structures: Applications to exploration problems. Society of Exploration Geophysicists.
- Farouk, S., Sen, S., Pigott, J. D., & Sarhan, M. A. (2022). Reservoir characterization of the middle Miocene Kareem sandstones, Southern Gulf of Suez Basin, Egypt. *Geomechanics and Geophysics for Geo-Energy and Geo-Resources*, 8(5), 130.
- Gluyas, J., & Swarbrick, R. (2004). *Petroleum geoscience* (p. 349). Blackwell Science.
- Goovaerts, P. (1997). *Geostatistics for natural resources evaluation*. Oxford University Press on Demand.
- Hempton, M. R. (1987). Constraints on Arabian plate motion and extensional history of the Red Sea. *Tectonics*, 6(6), 687–705.
- Hu, L. Y., & Ravalec-Dupin, M. L. (2005). On some controversial issues of geostatistical simulation. In O. Leuangthong & C. V. Deutsch (Eds.), *Geostatistics Banff 2004. Quantitative geology and geostatistics*. (Vol. 14). Springer.
- James, N. P., Coniglio, M., Aissaoui, D. M., & Purser, B. H. (1988). Facies and geologic history of an exposed Miocene rift-margin carbonate platform: Gulf of Suez, Egypt. *AAPG Bulletin*, 72(5), 555–572.
- Kassem, A. A., Sharaf, L. M., Baghdady, A. R., & El-Naby, A. A. (2020). Cenomanian/Turonian oceanic anoxic event 2 in October oil field, central Gulf of Suez, Egypt. *Journal of African Earth Sciences*, 165, 103817.
- Khalil, S. M. (1998). Tectonic evolution of the eastern margin of the Gulf of Suez. Egypt PhD Thesis Royal Holloway, University of London (p. 349).
- Mahmoud, A. I., Metwally, A. M., Mabrouk, W. M., & Leila, M. (2023). Controls on hydrocarbon accumulation in the pre-rift paleozoic and late SYN-rift cretaceous sandstones in PTAH oil field, north Western Desert, Egypt: Insights from seismic stratigraphy, petrophysical rock-typing and organic geochemistry. *Marine and Petroleum Geology*, 155, 106398.
- Mostafa, A., Sehim, A., & Yousef, M. (2015). Unlocking subtle hydrocarbon plays through 3D seismic and well control: A case study from West Gebel El Zeit district, southwest Gulf of Suez, Egypt. In *Offshore mediterranean conference and exhibition*. OnePetro.
- Moustafa, A. M. (1976). Block faulting in the Gulf of Suez. In *Proceedings of the 5th Egyptian general petroleum corporation exploration seminar, Cairo, Egypt* (Vol. 35).
- Nabawy, B. S., & Barakat, M. K. (2017). Formation evaluation using conventional and special core analyses: Belayim Formation as a case study, Gulf of Suez, Egypt. *Arabian Journal of Geosciences*, 10, 1–23.
- Nanda, N. C., & Nanda, N. C. (2016). Seismic wave propagation and rock-fluid properties. *Seismic Data Interpretation and Evaluation for Hydrocarbon Exploration and Production: A Practitioner's Guide*, 8, 3–17.
- Nouredin, A. M., Mabrouk, W. M., Chikiban, B., & Metwally, A. (2023b). Formation evaluation utilizing a new petrophysical automation tool and subsurface mapping of the Upper Cretaceous carbonate reservoirs, the southern periphery of the Abu-Gharadig basin, Western Desert, Egypt. *Journal of African Earth Sciences*, 205, 104977.
- Nouredin, A. M., Mabrouk, W. M., & Metwally, A. M. (2023a). Superimposed structure in the southern periphery of Abu Gharadig Basin, Egypt: Implication to petroleum system. *Contributions to Geophysics and Geodesy*, 53(2), 97–110.
- Nouredin, A. M., Mabrouk, W. M., & Metwally, A. (2023c). Delineating tidal channel feature using integrated post-stack seismic inversion and spectral decomposition applications of the upper cretaceous reservoir Abu Roash/C: A case study from Abu-Sennan oil field, Western Desert, Egypt. *Journal of African Earth Sciences*, 205, 104974.
- Nouredin, M. A., Walid, M. M., & Metwally, A. (2023d). Structural and petroleum system analysis using seismic data interpretation techniques to Upper Cretaceous rock units: A case study, West Abu-Sennan oil field, Northern Western Desert, Egypt. *Journal of African Earth Sciences*, 198, 104772.
- Okeil, M., Sakran, S., Refaat, A., El-Gamil, S., & Ramzy, M. (2019). Integrated geological interpretation for modeling the complicated reservoirs; An example from Upper Rudeis and Kareem Reservoirs, Amal Field, Southern Gulf of Suez Rift, Egypt. *Egyptian Journal of Geology*, 63, 101–114.
- Poupon, A., & Leveaux, J. A. C. Q. U. E. S. (1971). Evaluation of S_w in shaly formations. In *SPWLA 12th annual logging symposium*. OnePetro.
- Patton, T. L., Moustafa, A. R., Nelson, R. A., & Abdine, S. A. (1994). Tectonic evolution and structural setting of the Suez rift: chapter 1: Part I. *Type basin: Gulf of Suez*.
- Radwan, A. E., Wood, D. A., Mahmoud, M., & Tariq, Z. (2022). Gas adsorption and reserve estimation for conventional and unconventional gas resources. In *Sustainable geoscience for natural gas subsurface systems* (pp. 345–382). Gulf Professional Publishing.
- Radwan, A. E. (2022). Three-dimensional gas property geological modeling and simulation. In *Sustainable geoscience for natural gas subsurface systems* (pp. 29–49). Gulf Professional Publishing.
- Radwan, A. E., Abdelghany, W. K., & Elkhawaga, M. A. (2021). Present-day in-situ stresses in Southern Gulf of Suez, Egypt: Insights for stress rotation in an extensional rift basin. *Journal of Structural Geology*, 147, 104334.
- Radwan, A. E., Abudeif, A. M., Attia, M. M., & Mohammed, M. A. (2019). Pore and fracture pressure modeling using direct

- and indirect methods in Badri Field, Gulf of Suez, Egypt. *Journal of African Earth Sciences*, 156, 133–143.
- Radwan, A. E., Kassem, A. A., & Kassem, A. (2020). Radwany Formation: A new formation name for the Early-Middle Eocene carbonate sediments of the offshore October oil field, Gulf of Suez: Contribution to the Eocene sediments in Egypt. *Marine and Petroleum Geology*, 116, 104304.
- Ramadan, M. A. M., Abd El Hamed, A. G., Badran, F., & Nooh, A. Z. (2019). Relation between hydrocarbon saturation and pore pressure evaluation for the Amal Field area, Gulf of Suez, Egypt. *Egyptian Journal of Petroleum*, 28(1), 1–9.
- Said, R. (1990). *Geology of Egypt* (p. 743). A. A. Balkema. <https://doi.org/10.1017/S0016756800019828>.
- Shehata, A. A., Kassem, A. A., Brooks, H. L., Zuchuat, V., & Radwan, A. E. (2021). Facies analysis and sequence-stratigraphic control on reservoir architecture: Example from mixed carbonate/siliciclastic sediments of Raha Formation, Gulf of Suez, Egypt. *Marine and Petroleum Geology*, 131, 105160.
- Stephens, D. B., Hsu, K. C., Prieksat, M. A., Ankeny, M. D., Blandford, N., Roth, T. L., & Whitworth, J. R. (1998). A comparison of estimated and calculated effective porosity. *Hydrogeology Journal*, 6, 156–165.
- Wu, Q., & Xu, H. (2004). On three-dimensional geological modeling and visualization. *Science in China Series D: Earth Sciences*, 47, 739–748.
- Yan-lin, S., Ai-ling, Z., You-bin, H., & Ke-yan, X. (2011). 3D geological modeling and its application under complex geological conditions. *Procedia Engineering*, 12, 41–46.
- Zhang, T. F., Tilke, P., Dupont, E., Zhu, L. C., Liang, L., & Bailey, W. (2019). Generating geologically realistic 3D reservoir facies models using deep learning of sedimentary architecture with generative adversarial networks. *Petroleum Science*, 16, 541–549.